Quarterly Reviews of Biophysics **43**, 2 (2010), pp. 185–217. © Cambridge University Press 2010
doi:10.1017/S0033583510000107 Printed in the United States of America

Insight into helicase mechanism and function revealed through single-molecule approaches

Jaya G. Yodh[1], Michael Schlierf[1] and Taekjip Ha[1,2]*

[1] Department of Physics and Center for the Physics of Living Cells, University of Illinois at Urbana-Champaign, Urbana, IL, USA
[2] Howard Hughes Medical Institute, University of Illinois at Urbana-Champaign, Urbana, IL, 61801 USA

Abstract. Helicases are a class of nucleic acid (NA) motors that catalyze NTP-dependent unwinding of NA duplexes into single strands, a reaction essential to all areas of NA metabolism. In the last decade, single-molecule (sm) technology has proven to be highly useful in revealing mechanistic insight into helicase activity that is not always detectable via ensemble assays. A combination of methods based on fluorescence, optical and magnetic tweezers, and flow-induced DNA stretching has enabled the study of helicase conformational dynamics, force generation, step size, pausing, reversal and repetitive behaviors during translocation and unwinding by helicases working alone and as part of multiprotein complexes. The contributions of these sm investigations to our understanding of helicase mechanism and function will be discussed.

1. Introduction 186

2. Single-molecule techniques used to probe helicase function 188
2.1. Total Internal Reflection (TIR) and confocal smFRET 188
2.2. Flow-induced DNA stretching 190
2.3. Magnetic tweezers 192
2.4. Tethered particle assay (TPA) 192
2.5. Optical tweezers 193
2.6. Atomic force microscopy 193

3. Helicase questions addressed through single-molecule investigations 194
3.1. Scope of review 194
3.2. Active versus passive unwinding 194
3.2.1. Defining active and passive modes of unwinding 194
3.2.2. Hepatitis C virus NS3 helicase 195
3.2.3. Phage T7 replicative helicase 195
3.2.4. Phage T4 gp41 helicase 196
3.2.5. Implications for helicase mechanisms 196
3.3. Step size for helicase unwinding and translocation 197
3.3.1. Step-size definitions and measuring techniques 197
3.3.2. SFI helicases UvrD and PcrA 198
3.3.3. Replicative RNA helicases 199

* Author for Correspondence: Dr. T. Ha, Department of Physics and Center for the Physics of Living Cells University of Illinois at Urbana-Champaign, 1110 West Green St., Urbana, IL 61801, USA. Tel.: 217-244-0717; Fax: 217-244-7187; Email: tjha@illinois.edu

https://doi.org/10.1017/S0033583510000107 Published online by Cambridge University Press

3.3.4. Implications for helicase mechanisms 200
3.4. Pausing, reversal and repetition during helicase activity 201
3.4.1. Pausing and reversal by RecBCD 201
3.4.2. Force-dependent unwinding/rewinding bursts by UvrD and replicative helicases 203
3.4.3. Reverse motions during helicase activity detected by smFRET 205
3.5. Conformational dynamics during helicase activity 206
3.5.1. Repetitive shuttling during translocation 206
3.5.2. Replicative helicase–DNA tail interaction dynamics 207
3.5.3. DEAD-Box RNA helicase conformational switching 208
3.6. Helicases working in multiprotein complexes 208
3.6.1. Phage T4 primosome assembly 209
3.6.2. Phage T7, T4 and *E. coli* replisome dynamics 209
3.6.3. Effect of human Replication Protein A (hRPA) on BLM unwinding dynamics 212
3.6.4. Translocation on hRPA-coated DNA by archaeal XPD helicase 212

4. Conclusions and future directions 213

5. Acknowledgements 213

6. References 213

1. Introduction

Helicases are enzymes that catalyze the NTP-dependent unwinding of duplex nucleic acids (NAs) into single strands (Fig. 1). This activity is ubiquitous in all pathways of NA metabolism ranging from DNA replication, repair and recombination to transcription, splicing and translation. DNA helicases and certain viral RNA helicases possess three intrinsic activities: NA-dependent NTP hydrolysis, NTPase-powered unidirectional translocation along single-stranded NA (ssNA), and NTPase-dependent unwinding of duplex NA. These helicases can be thought of as NA motors that translocate along ssNA and upon reaching an ssNA–double-stranded NA (dsNA) junction, continue to move through and separate the duplex. An exception, however, is RNA helicases in the DEAD-box classification which perform local strand separation induced upon NTP-dependent binding of helicase to RNA with limited NTP hydrolysis required for enzyme recycling (Chen *et al.* 2008; Hilbert *et al.* 2009; Liu *et al.* 2008). Helicases have been classified into six superfamilies (SFI–VI) based on conserved sequence motifs characteristic of proteins that catalyze directional translocation on NA. SFI and SFII helicases generally operate as monomers or dimers on a diverse range of DNA and RNA substrates, while SFIII–SFVI helicases adopt hexameric structures and function in replication. All helicases utilize one of two NTP-binding catalytic domains: the RecA fold or the AAA+ fold. Helicase structure and activity have been the subject of several recent reviews (Berger, 2008; Enemark & Joshua-Tor, 2008; Lohman *et al.* 2008; Patel & Donmez, 2006; Pyle, 2008; Singleton *et al.* 2007).

It is important to distinguish *bona fide* helicases that actually catalyze duplex NA unwinding from other helicase-like proteins that possess the ability to translocate along NA but cannot actually separate the strands. Some examples of the latter class of DNA motors include restriction enzyme, EcoR1241, SWI/SNF chromatin remodelers and branch migration complex RuvAB. While single-molecule (sm) techniques have been applied to study the latter class of DNA motors (Hopfner & Michaelis, 2007; Lionnet *et al.* 2006), we will limit the scope of this review to *bona fide* helicases.

https://doi.org/10.1017/S0033583510000107 Published online by Cambridge University Press

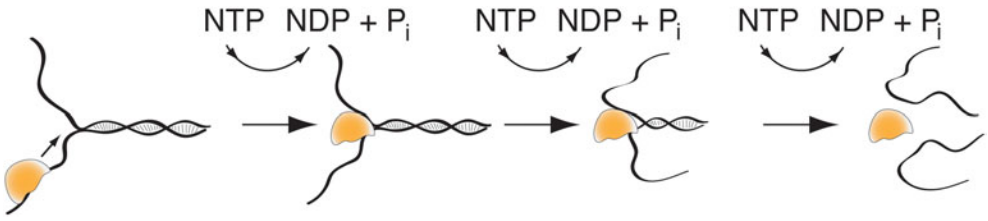


Fig. 1. Helicase activity involving translocation along ssNA: a helicase (yellow) will typically bind an ss region (for example the tail in the fork substrate shown) and use its intrinsic NTPase activity to translocate unidirectionally (either 3′–5′ or 5′–3′) along one of the single strands toward the ssNA–dsNA junction. Upon reaching the junction, the helicase will continue translocating and concurrently unwind the duplex into separate single strands, again powered by NTP hydrolysis.

NA melting/annealing in the absence of a protein catalyst is controlled by energy and entropic parameters. Melting is favored by conditions that result in higher entropic contribution to the free energy such as high temperature and the higher flexibility of single strands, whereas annealing is promoted by energetically favorable conditions that stabilize the duplex such as high ionic strength and GC content. As the cell cannot change its temperature or ionic environment, it relies on helicases to overcome the energetic barrier associated with base-pair melting. Under physiological conditions (8 mM ATP, 8 mM ADP and 0·4 mM P_i), the energy of NTP hydrolysis is 12·1 kcal/mol or $\sim 20\ k_B T$, which translates into 86 pN nm at 310 K (Phillips *et al.* 2008). For a maximally efficient helicase, then, unwinding 3–10 bp (i.e. moving $\sim$1–3·4 nm) translates into a maxmimal force generation of 25–86 pN. These estimates of helicase-induced force are in a range similar to experimental measurements of 10–20 pN force required to unzip NA in the absence of enzymes (Essevaz-Roulet *et al.* 1997). Another factor to consider regarding the physical work done by helicases is the role of NTP hydrolysis and its efficiency of utilization. If, for example, a helicase hydrolyzed one ATP per bp unwound, the $\sim 20\ k_B T$ of energy released would likely be amply sufficient to unwind a single bp ($\sim 3\ k_B T$ energy barrier per GC bp unwound) and also in many cases to power translocation along NA – all of which would require energy-dependent enzyme conformational changes. Such estimates help provide a theoretical framework for the physical parameters under which helicases operate, and thus guide experimental designs to probe helicase activity.

To date, a large body of knowledge on helicase structure, substrate specificity, kinetics and mechanisms of unwinding has been obtained through structural and ensemble-level studies (Lohman *et al.* 2008; Pyle, 2008; Singleton *et al.* 2007). More recently, sm approaches have been applied to probe mechanistic details and heterogeneity of helicase action that are undetectable by ensemble-averaged measurements (Hopfner & Michaelis, 2007; Lionnet *et al.* 2006; Rasnik *et al.* 2006). Optical/magnetic trapping/tweezer-based methods have yielded information about differences in force generation by helicases, step size of helicase movement along DNA, and detected pausing and reversal during helicase unwinding. smFRET-based methods have allowed observations of conformational dynamics in protein–NA and protein–protein interactions during translocation and unwinding, yielded data on helicase step size, and led to the discovery of repetitive behavior in helicase translocation and unwinding. Lastly, flow-stretch, tweezer-based and sm fluorescence methods have helped elucidate how helicases function in multiprotein complexes. The significant increase in our level of understanding and

https://doi.org/10.1017/S0033583510000107 Published online by Cambridge University Press

exploration of helicase mechanisms achieved through sm technology is the focus of the current review.

2. Single-molecule techniques used to probe helicase function

During the last several decades, ensemble studies have yielded considerable information on helicase function and mechanism. Among the most widely used techniques for measuring unwinding in bulk are gel electrophoresis-based monitoring of complete unwinding of radioactively labeled NA substrates as well as fluorimeter-based measurement of unwinding of fluorescently labeled substrates. These assays have helped elucidate helicase functional properties regarding substrate specificity and steady-state kinetic parameters. Adaptation of these assays to stopped-flow technology has allowed for measurement of unwinding under single-turnover conditions providing more accurate measurement of translocation step size and unwinding kinetics in a synchronized ensemble population (see section 3.3.1 for more details). These bulk techniques, however, are not able to detect unwinding reaction intermediates or any heterogeneity in activity within the population. In contrast, sm techniques can be used to observe reaction dynamics in real time, discover novel behaviors, and evaluate force dependence of the activities of this class of enzymes.

The last decade has witnessed the emergence of a variety of sm techniques and their rapid adoption for biophysical inquiries. On the one hand, sm force spectroscopy with atomic force microscopy (AFM) and optical/magnetic tweezers allows for the manipulation and observation of force-induced mechanical changes, yielding important information about the energy landscape of NA and protein–NA interactions. These studies perturb the free energy landscape of single molecules with force such that certain reactions are sped up or slowed down to mimic intracellular forces or to match the experimentally observable time scale. On the other hand, sm fluorescence and sm Förster resonance energy transfer (smFRET) are tools to watch relatively unperturbed molecular dynamics on the length scale of 2–8 nm (Roy, Hohng & Ha, 2008). Currently, smFRET is typically used to study protein–NA interactions, protein folding and enzyme kinetics (Roy *et al.* 2008). These investigations observe NTP-dependent conformational changes, equilibrium fluctuations or the relaxation of individual molecules after a perturbation of their equilibrium. In this section, we will survey sm techniques that have been applied to helicase studies (Fig. 2 and Table 1). Our goal is to provide an overview of how and why these techniques are employed in specific examples that will be discussed further in section 3.

2.1 Total Internal Reflection (TIR) and confocal smFRET

Figure 2*a* illustrates a typical design of a surface-tethered smFRET helicase study. For this assay, it is crucial to ensure that the protein interacts as little as possible with the surface; thus, several protocols for surface passivation have been developed. In the example shown, a glass surface is covered with polyethylenglycol (PEG) to reduce non-specific protein–surface interactions. The specificity is then provided by biotinylated-PEG to ensure NA tethering at a desired surface density via a highly specific biotin–avidin interaction. Typically the donor (green) and acceptor (red) are attached at the junction of the illustrated fork structure. Once a helicase (yellow) starts to open the dsNA, the donor gradually separates from the acceptor, with a corresponding reduction in FRET efficiency. FRET efficiency is a measure of how efficiently energy is transferred from the excited donor to the acceptor. Since FRET is due to a dipole–dipole interaction,

https://doi.org/10.1017/S0033583510000107 Published online by Cambridge University Press

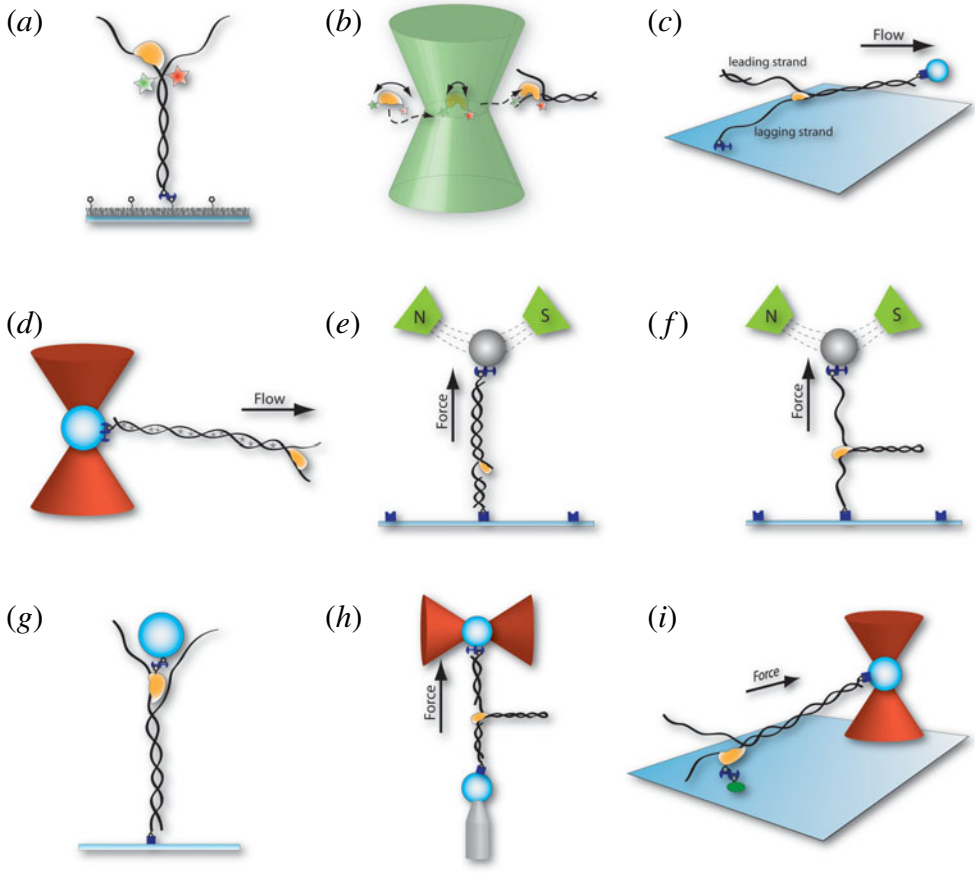


Fig. 2. Single-molecule techniques used to probe helicase function. (*a*) TIR smFRET: smFRET is used in surface-tethered assays such that dsNAs are specifically attached to a passivated surface via biotin–streptavidin interaction. Time traces of individual helicases converting dsNA (with donor and acceptor initially in close proximity) to ssNA are obtained over tens of seconds via EMCCD cameras and total internal reflection (TIR) illumination. (*b*) Confocal smFRET: alternatively, single helicase molecules can be dual-labeled with donor and acceptor, and cofactor-induced conformational changes can be monitored by confocal microscopy of individual diffusing molecules. (*c*) Flow-stretch method: in flow-stretch experiments dsDNA is stretched via laminar flow while attached to the surface. The extension of the stretched DNA is monitored using light microscopy to follow a microsphere attached to the other end of the surface-tethered dsDNA. The molecular elasticity of dsDNA is significantly different from that of ssDNA and thus the conversion of dsDNA to ssDNA results in a shortening or lengthening of the extension. (*d*) Flow stretch with optical tweezers: a derivative flow-stretch experiment follows the release of a dsDNA intercalator (illustrated as *) upon conversion of dsDNA to ssDNA. In this approach, the dsDNA is specifically attached to a microsphere held in solution by optical tweezers and stretched via laminar flow. (*e*) Magnetic tweezers (nicked linear substrate): here, DNA is specifically bound to the surface as well as a paramagnetic microsphere. Applying a magnetic field can stretch the DNA at a specific force. Again the conversion of dsDNA to ssDNA will lead to a change in the height of the microsphere above the surface at a constant force. This change can be monitored with light microscopy and converted to a length change from dsDNA to ssDNA. (*f*) Magnetic tweezers (hairpin substrate): alternatively magnetic tweezers can directly apply a force on an NA hairpin substrate and thus assist the helicase in opening of the duplex. dsNA opening is measured using light microscopy to follow microsphere height above the surface. (*g*) TPA: a force-free approach to monitor helicase activity in which the helicase is specifically bound to a microsphere and unwinding is monitored via light microscopy of the microsphere height above the surface. (*h*) Optical tweezers: optical tweezers offer the highest resolution and are most commonly used with a hairpin substrate to probe helicase activity. The dsNA hairpin is tethered between a microsphere and a surface/microsphere. Once the helicase opens the

https://doi.org/10.1017/S0033583510000107 Published online by Cambridge University Press

it is strongly distance-dependent. FRET efficiency is given by $E = \{1/[1 + (R/R_0)^6]\}$, with R the distance between the donor and acceptor and R_0 the characteristic distance for the energy transfer. R_0 depends on the choice of the fluorophores and their environment and is typically $\sim$50 Å. Thus, FRET is an excellent tool to track distance changes from 20 to 80 Å with a typical time resolution of 30 ms. Information regarding ssNA–dsNA junction binding and opening, mechanisms of unwinding and step size, for example, can be addressed with smFRET achieving a relatively high throughput (200–400 molecules in a typical imaging area) if smFRET data are taken with CCD cameras. Extremely fast processes can barely be captured with currently available sm CCD cameras, but can be recorded, for instance, molecule-by-molecule using confocal microscopy with single photon detectors (Roy *et al.* 2008). While local processivity of a few tens of bp can be studied well with smFRET, more processive helicase unwinding on templates of several hundred bp has only been studied in one case to date (Wickersham *et al.* 2010).

An alternative approach for smFRET is a non-tethered assay using confocal microscopy, as illustrated in Fig. 2*b*. Typically, the helicase is dual-labeled and thus conformational dynamics are probed. In this assay, the reaction buffer contains varying concentrations of cofactors and substrates, and FRET efficiency of individual molecules diffusing through the confocal volume is measured. The observation time is, however, limited by the diffusion of the molecule through the confocal volume ($\sim$0·1 ms). Hence, this smFRET technique does not monitor the trajectory of an individual molecule over time, but rather samples an ensemble average on a sm basis. The advantages of this technique over a more traditional ensemble assay are that singly-labeled molecules can be excluded from the analysis, that it allows for probing dimerization/multimerization effects, and that subpopulations can be detected.

2.2 Flow-induced DNA stretching

Flow-induced DNA stretching exploits the effect of laminar flow acting on a μm-sized bead to create controlled low stretching forces ($<$5 pN) on the attached DNA. Figure 2*c* shows a sketch of this tethered particle method. In this set-up, typically a 15–50 kbp long dsDNA substrate is used. The ends of this substrate are modified such that it specifically binds to the surface via a biotin modification at the lagging strand creating a replication fork-like structure. The other end of the dsDNA is modified for specific binding to the microsphere. In order to prevent non-specific interaction between the microsphere and the glass surface, a paramagnetic microsphere is used combined with a permanent magnet placed above the experimental flow cell. The data collection uses the elasticity/force–extension relationship of ssDNA and dsDNA. At forces below $\sim$5 pN, the extension of ssDNA is shorter than that of dsDNA. The helicase unwinding reaction that converts dsDNA into ssDNA is followed by monitoring the position of the microsphere, which comes closer to the tether point as more dsDNA is unwound. Although the spatial resolution of this assay is only on the order of 100 bp with 200–500 ms temporal resolution (50–100 molecules in parallel), it enables studies of helicases with high processivity and

pre-tensioned dsNA hairpin, the additional length results in a force decrease that can be compensated by a feedback system. In this configuration, the external force assists the helicase in unwinding the dsNA. (*i*) Optical tweezers (helicase surface-tethered): a different approach for optical tweezers requires the specific attachment of the helicase to a passivated surface. The dsNA molecule is attached to a microsphere held by optical tweezers. This assay allows the study of translocation and unwinding properties of helicases with force acting along the translocation direction. See text and Table 1 for further details.

https://doi.org/10.1017/S0033583510000107 Published online by Cambridge University Press

https://doi.org/10.1017/S0033583510000107 Published online by Cambridge University Press

Table 1. *Parameters for single-molecule methods used to probe helicase activity*

Technique	Temporal resolution	Spatial resolution	Throughput (molecules)	Force	Comments	Example reference(s)
TIR smFRET	30 ms	<3 bp	200–400	N.A.	Limited spatial range 2–8 nm	Myong *et al.* (2007)
Confocal smFRET	1 ms	<3 bp	>100	N.A.	No time trajectories of individual molecules	Theissen *et al.* (2008)
Flow-stretch method	500 ms	100 bp	>100	2–5 pN	Reconstitution of whole replisomes; study of processivity	Hamdan *et al.* (2007)
Flow-stretch + optical tweezers	300 ms	800 bp	1	0·2 pN	Reconstitution of whole replisomes; study of processivity	Bianco *et al.* (2001)
Magnetic tweezers	50 ms	10 bp	10–20	5–40 pN	Force method with moderate throughput	Dessinges *et al.* (2004), Lionnet *et al.* (2007), Sun *et al.* (2008)
TPA	200–500 ms	100 bp	>100	N.A.	Protein engineering allows specific targeting of protein subunits	Dohoney and Gelles (2001)
Optical tweezers	20 ms	Up to 1 bp	1	1–40 pN	Highest spatial resolution, but only 1 molecule at a time	Cheng *et al.* (2007), Johnson *et al.* (2007), Perkins *et al.* (2004)
AFM imaging	N.A.	1 nm	>50	N.A.	No trajectories; snapshots of trapped complexes	Henn *et al.* (2001)
AFM force spectroscopy	1 ms	>5 bp (force resolution limited)	1	15–100 pN	Low throughput; difficult cantilever functionalization	Marsden *et al.* (2006)

N.A., not applicable.

their binding partners. The reconstitution of multiple interaction partners within the replication machinery (>10 proteins, >1 MDa) is also possible (Lee *et al.* 2006).

Another flow-stretching scheme is illustrated in Fig. 2*d*. In this set-up, a long dsNA is specifically bound to a microsphere held by an optical trap. The dsDNA is stretched via linear flow forces on the order of 0·2 pN. At this force, dsDNAs are mostly extended, which can be verified by fluorescence microscopy with a dsDNA intercalator (i.e. YOYO). Unlike the previous flow experiment, dsDNA length is tracked by fluorescence decrease since the dsDNA intercalator binds with a higher affinity to dsDNA than ssDNA. This method provides a measurement of helicase unwinding with a temporal resolution of ∼300 ms and a spatial resolution of ∼800 bp; however, only one molecule at a time can be assayed (Bianco *et al.* 2001).

2.3 Magnetic tweezers

A high-resolution method for studying single helicases in action is provided by magnetic tweezers (Fig. 2*e*). Here, a dsDNA is tethered between the surface and a paramagnetic microsphere. By applying a constant stretching force to the DNA, the transition between dsDNA and ssDNA can be followed by imaging the magnetic microsphere under bright field microscopy. In contrast to flow experiments, the exerted force on the microsphere is generally kept above 5 pN, resulting in DNA lengthening instead of shortening upon DNA unwinding. Thus a helicase converting the dsDNA to ssDNA will result in a microsphere moving toward the magnets that can be studied with approximately 10 bp spatial and 50 ms temporal resolution. In this assay, external force does not directly help dsDNA unwinding if it is kept lower than the B–S transition force of dsDNA (Dessinges *et al.* 2004).

An alternative approach for monitoring helicase unwinding activity with magnetic tweezers is shown in Fig. 2*f*. Here, a hairpin is tethered to the surface and a paramagnetic microsphere via specific biotin–avidin and digoxigenin–antidigoxigenin interactions. Monitoring the microsphere's diffraction pattern allows tracking of the helicase unwinding activity because, as in the previous case, the percentage of ssDNA is changed over time. By changing the strength of the magnetic field, one can change the force acting on the hairpin and therefore change the amount of 'helping force' for the helicase. A spatial resolution of ∼10 bp and a temporal resolution of ∼50 ms together with a throughput of approximately 10–20 molecules per experiment enable a detailed, efficient study of helicase unwinding (Lionnet *et al.* 2007; Ramanathan *et al.* 2009).

2.4 Tethered particle assay (TPA)

Another approach to study single-helicase NA unwinding is termed the tethered particle assay (TPA), as illustrated in Fig. 2*g*. The helicase of interest is specifically tethered to a microsphere via a biotin–avidin interaction, while the substrate is bound to the glass surface via a digoxigenin–antidigoxigenin interaction. The microsphere position over time can be monitored by differential interference contrast video microscopy. Thus, the time trajectory of the average microsphere height above the surface can be recorded with a time resolution of 100–500 ms. Furthermore, this technique enables a large throughput since in the field of view at least 100 individual molecules can be studied at the same time. By specifically engineering biotinylation to individual subunits of helicase complexes, this technique can be used to probe the composition of functional unwinding complexes (Dohoney & Gelles, 2001).

https://doi.org/10.1017/S0033583510000107 Published online by Cambridge University Press

2.5 Optical tweezers

The last tethered particle method to introduce is the optical tweezers set-up. Optical tweezers thus far have been used in two ways to study single helicase unwinding. In the first case sketched in Fig. 2*h*, an NA hairpin is tethered to two microspheres. Typically one microsphere is held in a focused laser beam. This microsphere is used to monitor length and force changes on the NA hairpin. By moving the other microsphere that is held, in this case with a micropipette, closer or farther apart, the force acting on the hairpin can be varied. Instead of using a micropipette and a second microsphere, one could also tether the second end of the hairpin to a microscope slide. Both micropipette and microscope slide are in direct contact with the experimental set-up, and the resulting drift and vibration therefore limit the spatial resolution to a few bp (Cheng *et al.* 2007; Johnson *et al.* 2007). Recently, dual-trap optical tweezers with both microspheres held by a focused laser beam have completely decoupled the system of interest from the experimental set-up. These studies achieved a single bp resolution at 20 ms temporal resolution for the movements of RNA polymerase and a viral DNA packaging motor (Abbondanzieri *et al.* 2005; Moffitt *et al.* 2009).

In Fig. 2*i*, we show an alternative approach to use optical tweezers to study single helicase unwinding. In this case, the helicase is not free in solution for binding to the forked substrate, but is specifically bound to the microscope slide surface, for example, via a biotin–avidin bond. The forked substrate, on the other hand, is specifically bound to the microsphere that is held in the focused laser beam. Once a helicase starts unwinding, the force acting on the microsphere rises but can also be kept constant during the experiment. In using this approach, it is important to ensure that surface tethering of the helicase activity does not affect its activity. Since the force can be directly applied to the helicase translocation domains, a combined study of unwinding and translocation is the most likely outcome in this case. Any additional force applied in this case will most likely not assist in opening the dsNA. The resolutions are on the order of a few bp and 20 ms (Perkins *et al.* 2004).

2.6 Atomic force microscopy

AFM has been used in two different configurations to study helicase activity at the sm level. The first approach has been to use the high-resolution imaging capability of AFM (~1 nm/1 Å lateral/vertical resolution) to provide direct visualization of unwinding products by helicases. Bulk unwinding reactions are applied to the surface and dried, followed by imaging in air with ssNA easily distinguished from dsNA by the imaging height, while proteins attached to NA usually appear as 'blobs'. This method has been used to confirm ATP-dependent RNA unwinding by DEAD-box helicase DbpA (Henn *et al.* 2001), and to trap unwinding intermediates on plasmid DNA formed by PcrA in the presence of its initiator protein, RepD, SSB and ATP (Zhang *et al.* 2007). Direct imaging in air has also been applied to determine the UvrD dimer K_d via a quantitative volume AFM analysis method (Ratcliff & Erie, 2001).

AFM has also been used to measure helicase activity under force (pN resolution) using substrates tethered to the surface at one end and to the cantilever at the other end. This technique was applied to determine the force exerted by DEAD box protein 1 (Ded1) and eukaryotic initiation factor 4A/B (eIF4A/B) – RNA helicases involved in eukaryotic translation initiation – to unwind RNA stem loop structures (Marsden *et al.* 2006). Results showed that both helicases reduced the force required to unwind a 25 bp stem loop by ~35 pN; however, 3-fold less Ded1 was required to achieve this effect than eIF4A/B, consistent with the former's stronger

https://doi.org/10.1017/S0033583510000107 Published online by Cambridge University Press

ATPase activity. Despite these efforts, AFM only allows a coarse probe of helicase activity due to limitations in throughput and force resolution plus the inability to measure real-time kinetics and track enzyme motion (Table 1).

3. Helicase questions addressed through single-molecule investigations

3.1 Scope of review

As stated earlier, to limit the scope of this review, we will focus solely on *bona fide* helicases that catalyze NA duplex separation and exclude motors that translocate along NA but do not unwind it. The approach of this review will be to focus on the contributions of sm studies to the elucidation of major questions regarding helicase function and mechanism. We will focus on five major topics: (1) active versus passive unwinding, (2) step size of helicase translocation and unwinding, (3) pausing, reversal and repetition during helicase activity, (4) conformational dynamics during helicase activity and (5) helicases functioning in complexes with other proteins. For each topic, we will present case studies that illustrate how sm techniques have been utilized to reveal insights into these questions.

3.2 Active versus passive unwinding

3.2.1 Defining active and passive modes of unwinding

The mechanistic coupling of ssNA translocation to NA unwinding has been described in terms of two extreme cases – passive and active unwinding (Delagoutte & von Hippel, 2001; Lohman & Bjornson, 1996; Singleton & Wigley, 2002). A purely passive helicase will not enter the duplex region until thermal fluctuations cause the NA at the junction to open. The passive helicase can then move forward through the duplex by binding to the newly available ssNA, preventing it from reannealing. Thus, a purely passive helicase should translocate on ssNA faster than it can unwind the duplex. In contrast, a purely 'active' helicase is able to directly destabilize duplex NA at the junction by lowering its free energy such that the unwinding rate for a maximally active helicase would be expected to match its translocation rate on ssNA. A mathematical description of helicase activity in terms of active and passive unwinding has been developed (Betterton & Julicher, 2003, 2005) in which the degree of activeness ideally follows a scale of free energy reductions per bp unwound, ΔG_d (d refers to destabilization), induced by the helicase from 0 k_BT for a purely passive helicase to 3·4 k_BT (i.e. G–C base-pairing energy) for an optimally active helicase.

To date, tweezers-based assays on three different helicases (Cheng *et al.* 2007; Johnson *et al.* 2007; Lionnet *et al.* 2007) have yielded information on the range of activeness in helicase-promoted unwinding by analyzing the dependence of unwinding kinetics on NA sequence and external force. As the larger bond energy of G–C versus A–T/U base pairs can influence both thermal fraying of ends as well as duplex destabilization, sequence-dependence of unwinding velocity is expected for both active and passive cases. Increasing force is predicted to increase the unwinding rate to a larger extent for an initially passive helicase. The experimentally measured effects of these variables on unwinding kinetics were interpreted in terms of the aforementioned theoretical model (Betterton & Julicher, 2005). Results show that helicase unwinding mechanisms range from the highly active case of hepatitis NS3 helicase (Cheng *et al.* 2007) to the partially

https://doi.org/10.1017/S0033583510000107 Published online by Cambridge University Press

active phage T7 gp4 helicase (Johnson *et al.* 2007) to the mostly passive phage T4 gp41 helicase (Lionnet *et al.* 2007).

3.2.2 Hepatitis C virus NS3 helicase

Bustamante and co-workers (Cheng *et al.* 2007) used optical tweezers to investigate sequence- and force-dependence of unwinding of an RNA hairpin substrate by NS3 helicase. The hairpin contained a 60 bp duplex region that was either 30 GC followed by 30 AU or vice versa, and was tethered at both ends at constant tension, such that an increase in the length of the DNA/RNA handles was measured upon helicase-promoted unwinding (set-up similar to Fig. 2*b*). Consistent with their previous study (Dumont *et al.* 2006), the unwinding velocity was independent of force; however, a strong sequence-dependence of unwinding rate was observed at multiple forces (7 and 17 pN) with pausing upon encountering a sequence barrier (i.e. GC stretch). When the measured NS3 stepping velocity was compared to that expected for a passive helicase, it was 14 000-fold faster for unwinding on a GC template (assuming 4 bp unwinding per step (Dumont *et al.* 2006)), which translates into $\Delta G_d = 2{\cdot}5\ k_B T$. These observations indicate that NS3 unwinds actively, and does not wait passively for thermal fraying to occur before stepping. These results are summarized in an active duplex destabilization model that invokes barrier sensing by NS3 followed by strand separation occurring in sub-steps via an inchworm-type mechanism. An smFRET study on NS3 (Myong *et al.* 2007) suggested that DNA translocation in single nt steps leads to the accumulation of tension in the protein such that near-simultaneous unwinding of several bp occurs rapidly once enough elastic energy has built up. This study might help explain the observed force-independence of unwinding for NS3 (Dumont *et al.* 2006).

3.2.3 Phage T7 replicative helicase

Wang and co-workers (Johnson *et al.* 2007), reviewed in Ha (2007) used optical trapping to investigate the nature of unwinding by phage T7 replicative hexameric ring-shaped helicase in a set-up similar to Fig. 2*b*. Discrete measurements of ssDNA translocation as well as duplex DNA unwinding were made under constant tension, with translocation occurring faster than unwinding at low forces. As with the NS3 study (Cheng *et al.* 2007), a periodic sequence dependence of unwinding rate was observed corresponding to the positioning of pseudo-repeat sequences in the template, indicating that high GC content presents a barrier to unwinding. However, in contrast to NS3, the T7 helicase unwinding rate increased 10-fold, approaching the ssDNA translocation rate, as force was increased from 5 to 11 pN. This was paralleled by a corresponding increase in total unwinding distance (i.e. processivity). While these results appear to suggest that T7 helicase is intrinsically passive and external force allows it to become more active, the force dependence of unwinding rate was best fit by a hybrid active–passive model with $\Delta G_d = 1\text{–}2\ k_B T$ per bp that assumes a translocation step size of 2–4 nt and takes into account the measured ssDNA translocation rate, ssDNA elasticity and mechanical stability of the dsDNA. The increase in unwinding rate with force parallels previous findings in which the presence of DNA polymerase also speeds up unwinding (Lee & Yang, 2006; Stano *et al.* 2005), suggesting that one mechanism by which polymerases improve helicase processivity is by mechanically preventing negative regulation of the helicase by the unwound 3′ strand at the fork (Ha, 2007).

https://doi.org/10.1017/S0033583510000107 Published online by Cambridge University Press

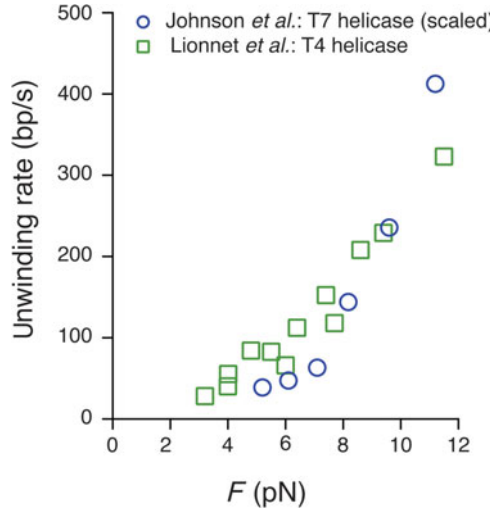


Fig. 3. Degree of activeness in helicase activity probed by single-molecule force techniques. Overlay of rescaled data of the ring-shaped helicases of T4 and T7 phages. Unwinding rate *versus* force for T7 helicase (Johnson *et al.* 2007) was rescaled to match the force-free unwinding rate of T4 helicase (28·4 bp/s) (Lionnet *et al.* 2007). The plot indicates that below 7 pN, the unwinding by T4 helicase is slightly more force dependent relative to T7 helicase, whereas, above 7 pN, T7 helicase unwinding is more sensitive to external force. See text for further details.

3.2.4 Phage T4 gp41 helicase

Another study on a replicative hexameric helicase, gp41 of phage T4 (Lionnet *et al.* (2007), uses a magnetic tweezers set-up similar to that shown in Fig. 2*f* to measure unwinding of a DNA hairpin tethered between a glass surface and a magnetic bead. The measured unwinding rate was 10-fold slower than the ssDNA translocation rate (i.e. rezipping rate in this system) at 3 pN, but it increased 10-fold as force was increased to 11 pN. When the measured data were fit to the Betterton and Julicher model (Betterton & Julicher, 2005), a ΔG_d of 0·05 k_BT was obtained consistent with passive unwinding. These data support gp41 functioning via the strand exclusion mechanism proposed for ring-shaped hexameric replicative helicases (Donmez & Patel, 2006) and are also consistent with the low processivity of gp41 without the gp43 polymerase (Dong *et al.* 1996; Schrock & Alberts, 1996). The higher ΔG_d observed in the similar T7 system (Johnson *et al.* 2007) was postulated to be due to differences in DNA sequence and elasticity between the substrates used in the two studies (Lionnet *et al.* 2007). A direct comparison of the unwinding velocity force dependence for the two phage replicative helicases (Fig. 3) suggests that below 7 pN, the unwinding by T4 helicase is slightly more force dependent (i.e. shows a greater slope in the unwinding rate versus force curve) relative to T7 helicase, whereas, above 7 pN, T7 helicase actually displays greater force dependence (and thus passivity) relative to T4 gp41. One possibility for the opposite interpretation presented by the aforementioned research is that this may be due to differences in the theoretical modeling of the data; thus, careful attention must be paid to this aspect when interpreting such studies.

3.2.5 Implications for helicase mechanisms

A general implication from these studies is that how actively or processively a helicase can unwind is regulated by factors such as the DNA sequence and the presence of accessory proteins

https://doi.org/10.1017/S0033583510000107 Published online by Cambridge University Press

like DNA polymerase. These investigations may also provide a mechanistic distinction between structurally different helicase superfamilies. The non-ring-shaped SFI helicases UvrD, Rep and PcrA have been shown to translocate along ssDNA faster than they unwind duplex regions, indicating that the energy of base pairing is an unwinding barrier (Bertram *et al.* 2002; Brendza *et al.* 2005; Cheng *et al.* 2002; Dillingham *et al.* 2000; Fischer *et al.* 2004; Maluf *et al.* 2003; Myong *et al.* 2005) similar to the aforementioned studies on phage T7 and T4 SFIV hexameric ring-shaped replicative helicases (Johnson *et al.* 2007; Lionnet *et al.* 2007). The force-dependence of the unwinding rate, however, varies between superfamilies, with the T7 and T4 helicases being strongly force-dependent (Johnson *et al.* 2007; Lionnet *et al.* 2007), the non-ring-shaped SFII hepatitis NS3 helicase reported as force-independent (Dumont *et al.* 2006), and UvrD reported both as force-independent (Dessinges *et al.* 2004) and impeded by force (Sun *et al.* 2008). The force-independence of unwinding indicates that, in some cases, strand separation alone is not the rate-limiting step. These differences might indicate a mechanistic distinction in how and why these helicases slow down upon encountering the junction. One possibility is that the non-ring-shaped helicases may undergo a rate-limiting dimerization step in order to unwind (Brendza *et al.* 2005; Fischer *et al.* 2004; Ha *et al.* 2002; Maluf *et al.* 2003; Myong *et al.* 2005).

3.3 Step size for helicase unwinding and translocation

3.3.1 Step-size definitions and measuring techniques

One of the key mechanistic questions regarding helicases is elucidation of step size or how many bp/nt are unwound/translocated per NTP hydrolyzed, also referred to as chemical step size or NTP coupling ratio. Other definitions of step size include (1) physical step size or average distance moved by the motor each time it moves on the NA lattice and (2) kinetic step size – the average number of bp unwound (or nt translocated) between two successive rate-limiting steps in the unwinding or translocation cycle (assuming it consists of n sequential steps of identical rates). Kinetic step size is not necessarily equivalent to chemical step size or the physical distance translocated. For example, a kinetic step size of 3 bp/nt might reflect a series of fast translocation steps in 1 nt increments followed by a slow rate-limiting step such as a conformational change that occurs every 3 bp. Physical translocation could also occur in larger steps comprised of multiple steps with different step sizes (Fischer & Lohman, 2004; Lohman *et al.* 2008).

Four methods have been used to determine/estimate helicase step size:

1. Crystallography is used primarily to infer NTP coupling ratios by structural comparisons of helicase–DNA co-crystals in the nucleotide-bound form versus apo-form.
2. Ensemble multiple-turnover kinetics can be used to obtain NTP coupling ratios by comparing the steady-state rates of unwinding or translocation to the rates of NTP hydrolysis.
3. Ensemble pre-steady-state single-turnover kinetics of unwinding/translocation and NTP hydrolysis (described below) allow for more accurate determination of kinetic and physical step sizes and NTP coupling ratios under conditions where the helicase binds once and does not rebind.
4. Sm methods allow for the determination of kinetic and physical step sizes.

In ensemble pre-steady-state single-turnover assays for unwinding and translocation (reviewed in Fischer & Lohman, 2004; Lucius *et al.* 2003), the helicase and DNA substrate are allowed to form an initial complex and then ATP is added using a stopped-flow apparatus and translocation/unwinding is measured as a function of time. Single-round kinetics is usually ensured by the

https://doi.org/10.1017/S0033583510000107 Published online by Cambridge University Press

addition of a protein trap such as heparin or excess DNA substrate to prevent any dissociated enzyme from rebinding the substrate. Unwinding assays measure the release of radioactively labeled single strands from the duplex or the decrease in FRET between a donor and acceptor fluorophore pair situated in close proximity on opposing strands of duplex substrates of varying lengths (Lucius *et al.* 2003). Direct translocation assays monitor the arrival of a helicase at the end of a ssDNA by measuring protein-induced changes in the intensity of a fluorophore positioned at the end of ssDNAs of varying lengths (Dillingham *et al.* 2002). In addition, a single-turnover fluorescent-based ATPase assay performed as a function of DNA cofactor length (Dillingham *et al.* 2000; Tomko *et al.* 2007) allows for calculation of the ATP coupling ratio.

Bulk kinetic determination of helicase step size can vary due to differences, for instance, in helicase oligomerization state, usage efficiency of NTP hydrolyzed, enzyme pausing and solution conditions. In some cases, translocation step size is not equivalent to unwinding step size, and large steps comprised of smaller sub-steps have been measured for a given enzyme. Sm studies have helped resolve controversy in the literature regarding step sizes predicted by crystallographic and bulk kinetic studies. To explain this, we will focus on two examples: SFIA helicases PcrA/UvrD and SFII replicative RNA helicases such as HCV NS3.

3.3.2 SFI helicases UvrD and PcrA

Crystallographic studies suggest that the binding/hydrolysis of 1 ATP causes inchworm-like translocation along ssDNA in 1 nt increments for *Bacillus stearothermophilus* PcrA (Velankar *et al.* 1999), and unwinding and translocation in 1 bp/nt increments for *Escherichia coli* UvrD (Lee & Yang, 2006). In these examples, as crystal structures were obtained with monomeric species, the conclusion is that the small 1 bp stepping is achieved by helicase monomers.

In contrast, ensemble single-turnover kinetic assays performed on these helicases resulted in larger step sizes for unwinding and translocation. Pre-steady-state assays led to the determination of translocation kinetic step sizes of $\sim$4 nt for UvrD (Fischer *et al.* 2004; Tomko *et al.* 2007) and PcrA (Niedziela-Majka *et al.* 2007) and of unwinding kinetic step sizes of 4–6 bp for UvrD (Ali & Lohman, 1997) and 4 bp for PcrA (Yang *et al.* 2008). Although the step size for translocation and unwinding correlates for each helicase, the protein/DNA ratios and length of the ssDNA tail in substrates used in these studies along with numerous bulk kinetic studies suggest that translocation is performed by a monomeric species whereas unwinding requires dimerization (Ali *et al.* 1999; Fischer *et al.* 2004; Maluf *et al.* 2003; Yang *et al.* 2008).

Further support for a larger kinetic step size was obtained from an sm magnetic tweezers study of UvrD unwinding (Dessinges *et al.* 2004; set-up similar to Fig. 2*e*), in which statistical analysis of helicase-induced noise in unwinding burst kinetics yielded a kinetic step size for unwinding of $\sim$6 bp. However, due to the large force (35 pN) applied to the ends of the nicked substrate in this work, it is possible that this measurement actually represented a translocation kinetic step size (Fischer *et al.* 2004). This was also suggested in a later magnetic tweezers investigation that monitored UvrD unwinding of a hairpin substrate (Sun *et al.* 2008; set-up similar to Fig. 2*f*), in which the unwinding rate was 4-fold lower than that reported by Dessinges *et al.* (2004). In this second sm study on UvrD (Sun *et al.* 2008), a similar statistical fluctuation analysis to that of Dessinges *et al.* (2004) was applied to calculate an unwinding kinetic step size of 4·2 bp. Xi and co-workers also suggest, based on the non-exponential distribution of off-times between unwinding bursts, that a UvrD dimer catalyzes unwinding in their assay (Sun *et al.* 2008).

https://doi.org/10.1017/S0033583510000107 Published online by Cambridge University Press

The ATP coupling ratios for translocation calculated from single-turnover ATPase time courses in the presence of varying length oligonucleotides were ~1 nt/ATP hydrolyzed for PcrA (Dillingham *et al.* 2000) and also for UvrD (Tomko *et al.* 2007). Recently, an ATP coupling ratio for unwinding by PcrA in the presence of initiator protein RepD was determined to be 1 bp per ATP hydrolyzed via similar assays with linear partial duplex and plasmid substrates (Slatter *et al.* 2009). The differences between the small ATP coupling ratio predicted by crystallographic studies and single-turnover ATPase kinetics and the larger kinetic step size calculated from ensemble single-round pre-steady-state kinetics and sm studies suggest that these helicases move 1 nt/bp per ATP hydrolyzed with a rate-limiting step in translocation or unwinding occurring every 4 ATPase cycles.

3.3.3 Replicative RNA helicases

In our second example of replicative RNA helicases, an ATP coupling ratio of 1 bp unwound per ATP hydrolyzed has also been predicted based on comparison of ATP-bound and unbound crystal structures of four SFII RNA helicases, including HCV NS3 helicase (reviewed in Hopfner & Michaelis, 2007). However, similar to the SFIA helicase family, ensemble kinetic and sm studies have shown larger step sizes and unwinding bursts. Single-round pre-steady-state kinetic measurements of unwinding of dsRNA of different lengths by Vaccinia virus NPH-II revealed a 6 bp RNA unwinding kinetic step size (Jankowsky *et al.* 2000). A combination of ensemble steady-state and pre-steady-state kinetic measurements of NS3 unwinding of RNA of different lengths revealed both a physical and a kinetic step size for RNA unwinding of 18 bp (Serebrov & Pyle, 2004). A complementary sm approach using optical tweezers to monitor NS3 unwinding of RNA hairpins (Dumont *et al.* 2006) found that extension occurred with a physical step size for unwinding of ~11 bp that was independent of ATP concentration and force. However, the optical tweezers experiment also detected three smaller sub-steps of 3·6 bp within each physical step, suggesting that NS3 is not unwinding in a single motion but in discrete smaller motions coordinated and triggered by the ATPase cycle, consistent with ATP-dependence of the stepping velocity and duration of pauses between steps (Dumont *et al.* 2006) (Fig. 4*a*).

A separate smFRET-based assay of DNA unwinding by NS3 helicase (Myong *et al.* 2007) revealed unwinding of a partial duplex 18 bp DNA in 3 bp steps. Dwell time analysis of pause durations at each step was consistent with three irreversible steps that need to occur before 3 bp unwinding, indicating that the elemental step size within each 3 bp is 1 nt. This led to the development of a model that translocation occurs in 1 nt increments, building up tension in a 'spring-loaded' NS3 such that every 3 nt, unwinding occurs in 3 bp bursts (Myong *et al.* 2007). These sm studies thus provide a way to understand the 1 nt translocation coupling ratio predicted by crystal structures with respect to the larger 3·6 bp unwinding steps observed (Fig. 4*b*). However, what about the larger kinetic steps sizes of 11 and 18 bp previously observed (Dumont *et al.* 2006; Serebrov & Pyle, 2004)? In another series of pre-steady-state stopped flow experiments using RNA of varying lengths and sequence (Serebrov *et al.* 2009), the step size reduced from 18 to 11 bp upon lowering the ionic strength. The NS3 oligomeric state was correlated with the ionic strength used in the previous studies, with it operating as a monomer at low ionic strength (Dumont *et al.* 2006) but as a dimer at higher ionic strength (Serebrov & Pyle, 2004). As the smFRET study (Myong *et al.* 2007) also showed that NS3 remained associated with the unwound strand, Pyle and co-workers (Serebrov *et al.* 2009) then proposed that the 11 or 18 bp

https://doi.org/10.1017/S0033583510000107 Published online by Cambridge University Press

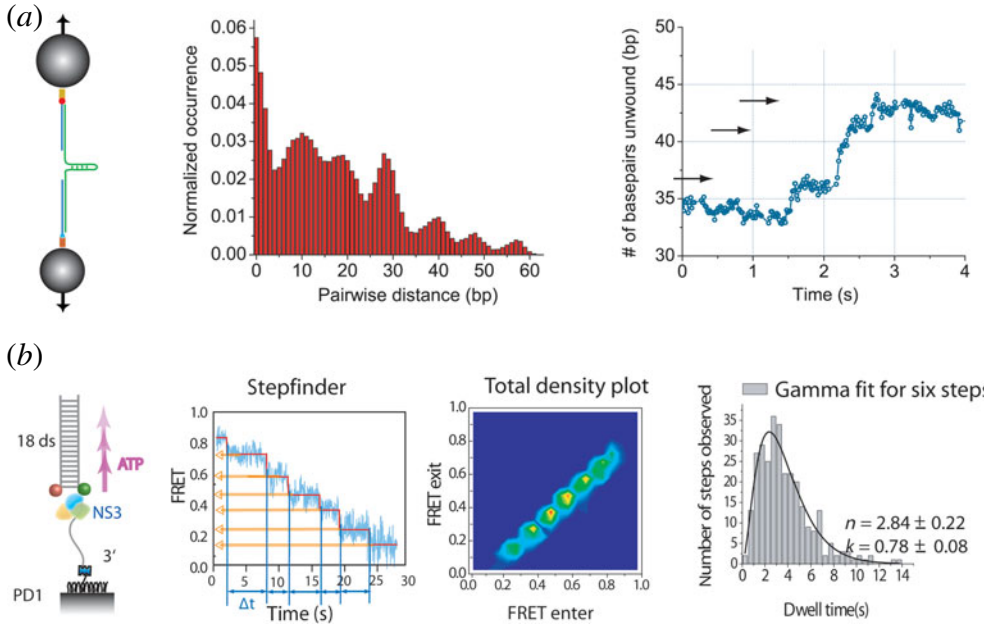


Fig. 4. Single-molecule studies on helicase step size: (*a*) From Dumont *et al.* (2006). (*Left*) Optical tweezer set-up to monitor NS3 helicase unwinding of an RNA hairpin (see Fig. 2*b*). (*Center*) Pairwise distance distribution for unwinding extension time traces reveals an 11 ± 3 bp periodicity in pausing during extension. (*Right*) Unwinding substeps of $3{\cdot}6 \pm 1{\cdot}3$ bp that appear within the 11 bp step observed at limiting ATP concentrations. Reprinted by permission from Macmillan Publishers Ltd: Nature *439*, 105–108, copyright (2006). (*b*) From Myong *et al.* (2007). (*Far left*) Experimental smFRET set-up to measure NS3 unwinding of 18 bp partial duplex DNA. (*Mid left*) FRET unwinding time trace fit to the step-finding algorithm quantitates FRET values and dwell times for six steps. (*Mid right*) Total density plot representing two-dimensional histograms for pairs of FRET values entering and exiting each transition reveals six peaks. (*Far right*) Gamma distribution fitting to collected dwell times at each plateau pause reveals three irreversible steps within the 3 bp step, indicating 1 nt elemental step size within each 3 bp transition. From Myong, S. *et al.* (2007) Science *317*, 513–516. Reprinted with permission from AAAS. See text for further details.

steps corresponded to 5′ unwound tail product release in pulses after RNA unwinding has reached a certain length.

3.3.4 Implications for helicase mechanisms

The combined work on NS3 provides evidence that helicases can move in 1 nt/bp steps which are linked to large conformational physical motions that occur during unwinding such as product release that are apparent as much bigger 'steps.' In general for all the helicases described, the smaller kinetic step sizes of 3–6 nt/bp that are observed through sm and pre-steady-state single-turnover kinetics represent ATP-dependent rate-limiting events such as unwinding bursts that occur after moving a discrete number of bp in single-nt increments. Nonlinear global fitting of the single-cycle kinetic ensemble data is limited by two factors: (i) the assumption that helicase movement occurs without slippage or pausing, which would lead to an overestimation of step-size (Fischer *et al.* 2004) and (ii) the uncertainty in step-size estimation caused by analyzing multiple datasets as a group (each with a limited amount of data) as opposed to a single dataset with less variation (Lucius *et al.* 2002). Both of these problems can be addressed by sm techniques,

https://doi.org/10.1017/S0033583510000107 Published online by Cambridge University Press

which in fact have detected pausing by many helicases (Lionnet *et al.* 2006) and derived kinetic information from datasets derived from single molecules (Myong *et al.* 2007, 2005).

3.4 Pausing, reversal and repetition during helicase activity

One of the advantages of sm measurements is that it allows for the detection of unsynchronized behavior of individual molecules such as enzyme and substrate conformational dynamics, chemical reaction intermediates and behavioral heterogeneity of individual molecules that normally would be masked in ensemble-averaged measurements. Examples of such behaviors revealed in sm investigations of helicases include enzyme pausing and reversal during translocation and unwinding. These findings have been made for a broad spectrum of helicases using a variety of sm techniques. We describe below how the discovery of these novel behaviors has provided insight into unwinding mechanisms and functions of several helicases.

3.4.1 Pausing and reversal by RecBCD

E. coli RecBCD is a dual helicase/nuclease required in recombinational repair of dsDNA breaks. The helicase initially binds at the break site and proceeds to unwind ~30 kbp using two motors, RecD and RecB, which translocate with opposite polarity. As it unwinds DNA, the enzyme degrades both strands at differential rates. Upon encountering a χ recombination hotspot, RecBCD undergoes a conformational change resulting in decreased helicase/nuclease activity and production of a long 3′ ss tail for loading of RecA and continuation of homologous recombination. The results of several sm studies have helped elucidate the mechanism and χ-site regulation of RecBCD translocation.

Two zero/low-force sm experimental systems have provided evidence for highly processive unidirectional movement by RecBCD along dsDNA. A tethered-particle-assay (TPA) investigation (Dohoney & Gelles, 2001) monitored changes in Brownian motion of a streptavidin-coated polystyrene bead linked to RecBCD through a biotin-tagged RecD as it unwound/degraded a 1 kb tethered DNA (in an assay similar to Fig. 2*g*). No enzyme pausing was detected regardless of whether the DNA contained an internal χ site, with RecBCD dissociating upon reaching the tether, thus ruling out a model where the χ-site-induced conformational change involves RecD subunit ejection. Another study (Bianco *et al.* 2001) used optical trapping fluorescence microscopy to measure RecBCD movement through 40-fold longer λ DNA (Fig. 2*d*). In this case, a small force was applied via the flow-stretch experimental set-up in order to stretch the long λ DNA. One end of the DNA was specifically attached to a microsphere and the dsDNA was visualized by YOYO fluorescence. A microfluidics set-up was used in which the DNA–RecBCD complex in one channel is captured in the optical trap and then moved to a second channel where ATP is flowed in. RecBCD unwinding/degradation was followed by monitoring changes in fluorescence while YOYO was released upon dsDNA shortening. Again, highly processive unwinding with no pausing was observed at saturating ATP over the length of the entire λ DNA.

This optical trapping fluorescence method was next applied to analyze RecBCD unwinding of 30 kb DNA containing χ sequences (Spies *et al.* 2003), and ~5 s χ-specific pauses were observed followed by unwinding at a reduced rate rate (Fig. 5*a*). This phenomenon was postulated to reflect either uncoupling of RecD from the holoenzyme or a conformational change in RecBCD that inactivates RecD. The detection of χ-induced pauses in this set-up as opposed to the TPA

https://doi.org/10.1017/S0033583510000107 Published online by Cambridge University Press

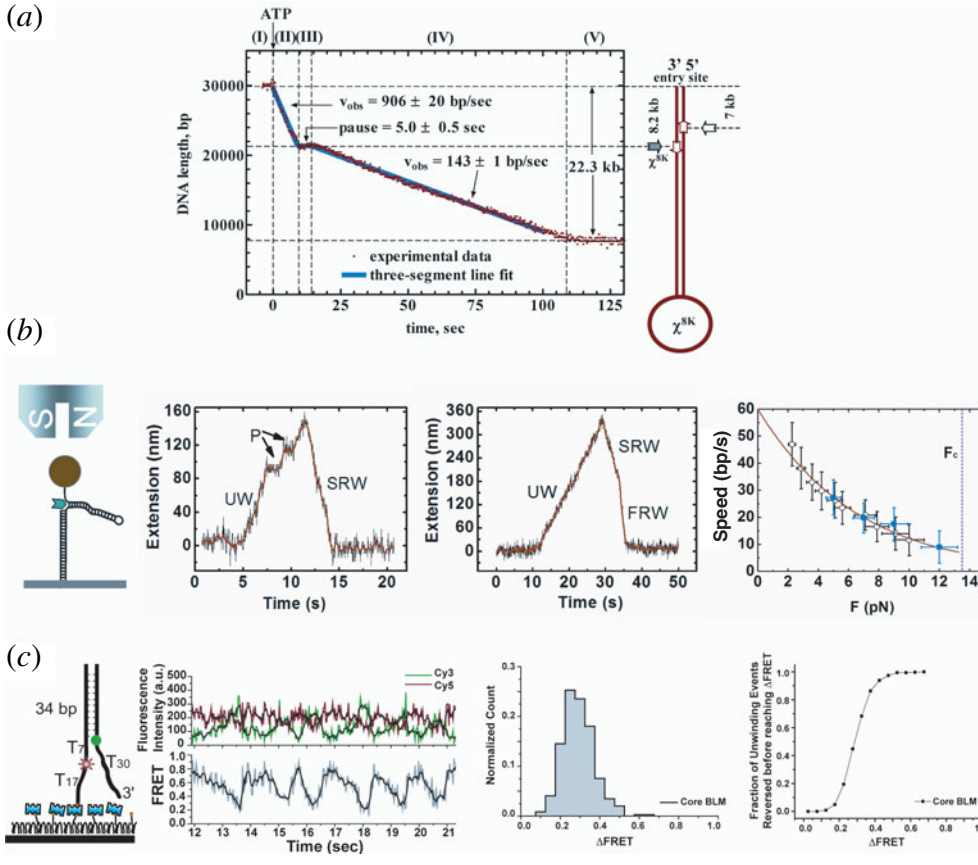


Fig. 5. Single-molecule detection of pausing and reversal during helicase unwinding. (*a*) From Spies *et al.* (2003). Optical trap fluorescence microscopy (see Fig. 2*d*) to monitor DNA unwinding by RecBCD detects χ-site-specific pausing followed by unwinding at a slower velocity by a RecD-uncoupled holoenzyme. Reprinted from Cell *114*, Spies, M. *et al.*, 'A molecular throttle: The recombination hotspot, χ controls DNA translocation by the RecBCD helicase,' Copyright (2003), with permission from Elsevier. (*b*) From Sun *et al.* (2008). Magnetic tweezers study of UvrD unwinding of DNA hairpin substrate (*far left*) shows multiple patterns in unwinding (UW) bursts followed by rapid rehybrization (not shown) or slower rewinding (SRW). (*Mid left*) Pauses (P) during unwinding may reflect transient dimer dissociation. (*Mid right*) Transitions from a slow to fast rewinding rate (FRW) may reflect dimer dissociation during translocation on the opposing strand after strand switching. (*Far right*) Inverse force dependence of unwinding rate was incorporated into a strained inchworm model for unwinding in which UvrD dimers bend the 3′ ssDNA tail to form an active unwinding species. Reprinted by permission from Macmillan Publishers Ltd: EMBO J. *27*, 3279–87, copyright (2008). (*c*) From Yodh *et al.* (2009). smFRET study of unwinding of forked DNA substrate (*far left*) by human BLM helicase. (*Mid left*) Example of partial repetitive unwinding behavior by a single helicase. (*Mid right*) Histogram of the change in FRET values in repetitive unwinding events shows a peak at 0·3 △FRET efficiency. (*Far right*) A threshold △FRET of 0·2 must be achieved before BLM reverses unwinding. These data suggest that BLM 'measures' the amount of bp it unwinds before it reverses unwinding. Reprinted by permission from Macmillan Publishers Ltd: EMBO J. *28*, 405–16, copyright (2009). See text for further details.

experiment was probably due to the higher spatiotemporal resolution. An extension of this experiment was performed without YOYO but instead using RecBCD tagged through its RecD subunit with a fluorescent bead (Handa *et al.* 2005). Again, processive unwinding was observed prior to a 6 s pause at the χ site, after which the unwinding rate decreased 2-fold. The fluorescent

https://doi.org/10.1017/S0033583510000107 Published online by Cambridge University Press

nanoparticle stayed with the RecBCD for the entire duration of the pause, thus agreeing with the conclusion made by Dohoney & Gelles (2001) that RecD is not dissociating at χ. Further analysis using the same assay with a RecBCD mutant with a non-functional RecD subunit (Spies *et al.* 2007) led to the finding that RecD is the lead motor prior to χ recognition whereupon RecD becomes uncoupled from the holoenzyme and RecB becomes the lead motor. The unwinding rates correlated with a model in which there is an initial requirement for fast unwinding of damaged or foreign DNA, but χ recognition signals the need to slow down in order to properly assemble the RecA filament.

As a follow-up to the original TPA study (Dohoney & Gelles, 2001), a force–TPA assay was developed in which a stretching force was applied by continuous laminar flow to the DNA–bead complex (Fan & Li, 2009). Using this force–TPA set-up with low ATP and 0·2 pN stretching force, RecBCD unwound a 4·1 kb DNA at the same rate observed previously, except in this case χ-specific pausing was observed followed by a rate decrease, suggesting that the lack of pausing seen by Dohoney & Gelles (2001) was likely due to the more limited resolution of that experimental set-up.

Block and co-workers applied a different force-based approach to investigate RecBCD activity (Perkins *et al.* 2004), in which a biotinylated RecBCD was tethered to a coverslip via a streptavidin linkage and a 7 kb DNA substrate lacking χ sites was attached at its distal end to a polystyrene bead held inside an optical trap over a varying force range as shown in Fig. 2*i*. The surface-bound enzyme bound to the free DNA end, and, upon ATP addition, its movement along dsDNA toward the trap, was monitored under constant force up to 8 pN. DNA unwinding correlated with decreasing length of the tether, and RecBCD was observed to move unidirectionally over ∼1000 s of bp. However, in contrast to the previous zero- or low-force studies (Bianco *et al.* 2001; Dohoney & Gelles, 2001), χ-independent pausing was observed, including transient force-dependent pauses as well as spontaneous pausing that was independent of both force and ATP. This high-resolution optical trapping method revealed yet another surprising behavior – sporadic uneven RecBCD-dependent backward movement during unwinding. Releasing the force converted the reversals into forward motions, indicating backsliding was caused by force. The change in tether length upon backsliding was consistent with partial ssDNA formation, indicating possibly an ssDNA loop formation after unwinding but prior to degradation. In general, the force-dependent pausing and reversal during RecBCD movement were not thought to be sequence-dependent but instead to reflect kinetically distinct persistent states of the enzyme–DNA complex.

3.4.2 Force-dependent unwinding/rewinding bursts by UvrD and replicative helicases

Magnetic tweezers studies of UvrD helicase have revealed pausing and reversal behavior (Dessinges *et al.* 2004; Sun *et al.* 2008). Croquette and co-workers (Dessinges *et al.* 2004) monitored the unwinding of an 11 kb singly nicked duplex DNA that was anchored to a magnetic bead at one end of the duplex and to a glass surface at the other end (as in Fig. 2*e*). At UvrD <1 nM, the extension versus time curves obtained at high force >30 pN exhibited isolated unwinding bursts. Each burst showed a regular increase in extension corresponding to unwinding. The slope and height of the burst were used to calculate the rate of unwinding (U) and extent of unwinding, respectively. Unwinding proceeded processively without pausing but occasionally the extension signal decreased back to baseline in one of two fashions – UH bursts showed an instantaneous decrease corresponding to enzyme dissociation and rapid

https://doi.org/10.1017/S0033583510000107 Published online by Cambridge University Press

rehybridization (H), whereas UZ bursts showed a much slower decrease reflecting a slower rezipping (Z) event. In UZ bursts, the slow rezipping rate was equivalent to the unwinding rate, and was ATP-dependent indicating that ssDNA translocation might be involved. These findings led the authors to propose a model in which UvrD is capable of reversing unwinding by switching strands and translocating 3′–5′ on the opposing single strand, thus inducing re-annealing behind the helicase. The high force required to achieve unwinding at low UvrD concentrations in this study most likely helps prevent reannealing during unwinding and was proposed to be the reason why unwinding is achieved at sub-nM concentrations unlike in bulk studies (Maluf *et al.* 2003).

A second study (Sun *et al.* 2008) analyzed force-dependent UvrD unwinding of a λ DNA hairpin situated between a λ dsDNA tethered to the surface and a 3′ ssDNA oligonucleotide tethered to a magnetic bead (similar to Fig. 2*f*). At saturating ATP, UvrD <10 nM and forces >4 pN, UvrD produced the UH and UZ unwinding burst patterns observed previously (Dessinges *et al.* 2004); however, additional patterns were also observed. First, pausing was observed in 25% of unwinding events during both U and Z phases as well as between them. The pausing frequency was inversely proportional to UvrD concentration, thus relating pausing to the enzyme oligomeric state. Second, slow and fast rezipping (Z) rates were observed, indicating there may be two kinds of translocases operating. The U and slow Z rates in the hairpin study (Sun *et al.* 2008) were 10-fold lower than those measured previously on nicked DNA (Dessinges *et al.* 2004), which were actually closer to the monomeric UvrD ssDNA translocation rate measured in ensemble studies (Fischer *et al.* 2004). The fast rezipping rate observed in the hairpin study was also closer to the ssDNA translocation rate. The distributions of off-times between unwinding bursts followed a non-exponential distribution that was inconsistent with single enzyme binding kinetics (Sun *et al.* 2008). In light of these findings, Xi and co-workers proposed that their unwinding bursts reflected unwinding by a dimeric helicase with the pausing representing transient or permanent dimer dissociation (Fig. 5*b*), which is reminiscent of the unwinding initiation and reinitiation model proposed for Rep helicase based on sm analysis (Ha *et al.* 2002). The switch between slow and fast rezipping may reflect dimer dissociation/monomer–monomer reassociation, with both dimers and monomers being able to switch strands and translocate on ssDNA (Sun *et al.* 2008).

Perhaps the most intriguing result of the second magnetic tweezers study (Sun *et al.* 2008) was that the UvrD unwinding rate *decreased* with increasing force, indicating that force kinetically impeded unwinding (Fig. 5*b*). From this the authors proposed that UvrD uses a strained inchworm mechanism for unwinding involving a UvrD dimer that must bend the 3′ ssDNA tail in order to achieve a modeled interaction of both 2B domains required for activation of unwinding. The experimental force on the ssDNA tail in this system may hinder the bending of the DNA at the junction and thus unwinding.

Croquette and co-workers also observed primarily UH/UZ-type events when monitoring unwinding of a hairpin substrate by T4 hexameric gp41 helicase via magnetic tweezers as shown in Fig. 2*f* (Lionnet *et al.* 2007) at saturating ATP, and forces between 6–10 pN. In UH events, the helicase unwound the hairpin fully and then dissociated, causing the hairpin to reanneal instantaneously. In UZ events, the slow rezipping phase was ATP-dependent, signifying helicase dependence; however, this was not caused by strand switching as proposed for UvrD (Dessinges *et al.* 2004) because the original substrate was a hairpin. Instead, the gp41 was proposed to continue translocating along the newly unwound DNA with the hairpin reannealing in its wake. Similar reverse motions characterized by unwinding/rewinding bursts have also been observed

https://doi.org/10.1017/S0033583510000107 Published online by Cambridge University Press

albeit infrequently for the T7 hexameric helicase using an optical trap-based unzipping assay at forces between 7 and 12 pN (Johnson *et al.* 2007). Finally, rare stepwise rewinding events have also been detected during NS3 unwinding of an RNA hairpin measured at 17 pN using an optical tweezers-based assay (Dumont *et al.* 2006).

3.4.3 Reverse motions during helicase activity detected by smFRET

smFRET studies on helicases have also revealed reverse motions and stalling during helicase activity at zero force. Initial studies on *E. coli* Rep helicase (Ha *et al.* 2002) using an unwinding substrate – a partial duplex DNA with both donor and acceptor dyes at the ssDNA–dsDNA junction (Fig. 2*a*) – revealed that Rep could efficiently unwind an 18 bp duplex but not a 40 bp duplex. Seventy percent of the time, unwinding of the 40-mer was punctuated by stalls that usually led to dissociation of Rep and reannealing of the substrate. The stalls were proposed to be due to dissociation of dimeric rep, the functional oligomeric state for unwinding. In some cases, reassociation of monomers led to unwinding reinitiation on the same substrate.

Ha and co-workers also discovered repeating unwinding patterns in smFRET time traces for two SFII helicases – HCV NS3 (Myong *et al.* 2007) and the human Bloom Syndrome helicase (BLM) helicase (Yodh *et al.* 2009). Using partial duplex DNA templates with a surface-tethered 18 bp duplex and acceptor and donor dyes situated at the junction on adjacent strands, the addition of ATP caused NS3 to unwind the DNA (with a corresponding FRET decrease); however, upon reaching the surface, the DNA reannealed instantaneously. This pattern was repeated in succession on the same molecule and persisted even after washing out free protein, indicating it was catalyzed by a single NS3 species. Incomplete, repetitive unwinding was also observed using duplexes longer than 18 bp, indicating that a steric blockade is not necessary for unwinding reversal. The authors proposed a model that NS3 remains in contact with the displaced strand during unwinding and, upon reaching a steric or length-based block, returns to the junction with concomitant strand reannealing and begins the unwinding cycle again (Myong *et al.* 2007).

Repetitive unwinding was also catalyzed by BLM helicase, a human RecQ homologue, on forked DNA of varying duplex lengths with the dyes situated in close proximity to the fork junction (Yodh *et al.* 2009) (Fig. 5*c*). This behavior was observed for wild-type BLM and a mutant comprising the RecQ catalytic core that lacks the oligomerization domain (Janscak *et al.* 2003). This fact as well as the protein concentration-independence of unwinding times led to the conclusion that successive unwinding events on the same DNA molecule are carried out by a single BLM monomer. Each unwinding event was characterized by three phases: (I) a phase during which FRET decreases by a certain amount, ΔFRET, due to unwinding, followed by (II) a time period during which FRET remains at a constant low value, followed by (III) a reannealing phase characterized by a rapid switch back to high FRET. The ATP-dependence of reannealing time was reminiscent of the ATP-dependence of the slow-rezipping events detected for UvrD previously (Dessinges *et al.* 2004). It was proposed that BLM partially dissociated after unwinding a critical length of DNA, and then switched its helicase motors to the opposing strand and translocated 3′–5′ on this strand with the strands reannealing in its wake. However, unlike UvrD and T7, which terminated unwinding stochastically after a random number of bp were unwound, BLM appeared to terminate after a short but defined length of DNA was unwound – based on a defined peak observed in ΔFRET distributions. Thus, BLM appears to be able to 'measure' the number of bp it has unwound, and once it has unwound a critical length, it rapidly reverses unwinding via strand switching (Fig. 5*c*). The ability to switch

https://doi.org/10.1017/S0033583510000107 Published online by Cambridge University Press

strands and measure DNA unwound may facilitate BLM processing of stalled replication forks and illegitimately formed recombination intermediates.

In these investigations on NS3 and BLM, smFRET was able to detect partially unwound intermediates in real time, leading to the discovery of repetitive unwinding. Repetitive behaviors during helicase translocation by Rep and RIG-I proteins (Myong *et al.* 2009; Myong *et al.* 2005) were also discovered using sm fluorescence (described in section 3.5).

3.5 Conformational dynamics during helicase activity

TPA and force-based tweezers techniques do not offer information on conformational changes in the enzyme or enzyme–substrate complexes during helicase action. In contrast, fluorescence-based sm techniques such as smFRET can detect conformational dynamics because of the ability to place donor and acceptor probes in specific locations on the enzyme and/or substrate and extract information regarding changes in probe–probe distances as the helicase operates in real time. In this section, we will describe smFRET investigations that have focused on helicase dynamics during translocation (Myong *et al.* 2005), substrate–enzyme binding dynamics (Rothenberg *et al.* 2007) and helicase interdomain arrangements (Aregger & Klostermeier, 2009; Karow & Klostermeier, 2009; Linden *et al.* 2008; Theissen *et al.* 2008).

3.5.1 Repetitive shuttling during translocation

smFRET was used to measure *E. coli* Rep translocation on ssDNA using a partial duplex substrate with acceptor dye positioned at the junction end of the 3′ ssDNA tail while the enzyme was donor-labeled (Myong *et al.* 2005). These experiments were performed at sub-nM concentrations of Rep that do not allow unwinding which requires more than a monomer of Rep. In the presence of ATP, ssDNA translocation by Rep was expected to initiate with the enzyme binding to the available 3′ end of the ssDNA tail producing a low FRET signal and then moving toward the junction with a corresponding FRET increase related to the distance translocated. However, the enzyme did not dissociate upon reaching the junction but instead appeared to snap back to the 3′ end of the ssDNA (observed as an abrupt FRET decrease), and showed repeated cycles of translocation and snap-back. The same phenomenon was observed with dual-labeled Rep and an unlabeled translocation substrate, indicating that Rep undergoes a conformational change during translocation from an open to closed form, possibly exposing a secondary binding site that then rebinds the free 3′ tail, transferring Rep from the junction back to the 3′ end of the ssDNA tail whence it begins another cycle (Fig. 6*a*). This translocation behavior was termed ‘repetitive shuttling’ and was proposed to play a role in the removal of proteins such as RecA filaments in order to prevent unwanted recombination. Note that Rep shuttling behavior was also observed using sm protein-induced fluorescent enhancement (PIFE) with unlabeled Rep on a Cy3-labeled DNA (Myong *et al.* 2009).

The PIFE technique was also applied to show that the dsRNA-dependent SFII DExH ATPase, RIG-I, a cytosolic viral sensor, can translocate on dsRNA in an ATP-dependent manner (Myong *et al.* 2009). Similar to Rep translocation along ssDNA, a single RIG-I catalyzed translocation in successive repetitions on the same RNA molecule. Although the physical mechanism of RIG-I dsRNA translocation is still unclear, the finding that this activity could be *trans*-activated by 5′ triphosphate caps that are typically present on viral RNA post-infection is consistent with a role for this activity in viral sensing by RIG-I.

https://doi.org/10.1017/S0033583510000107 Published online by Cambridge University Press

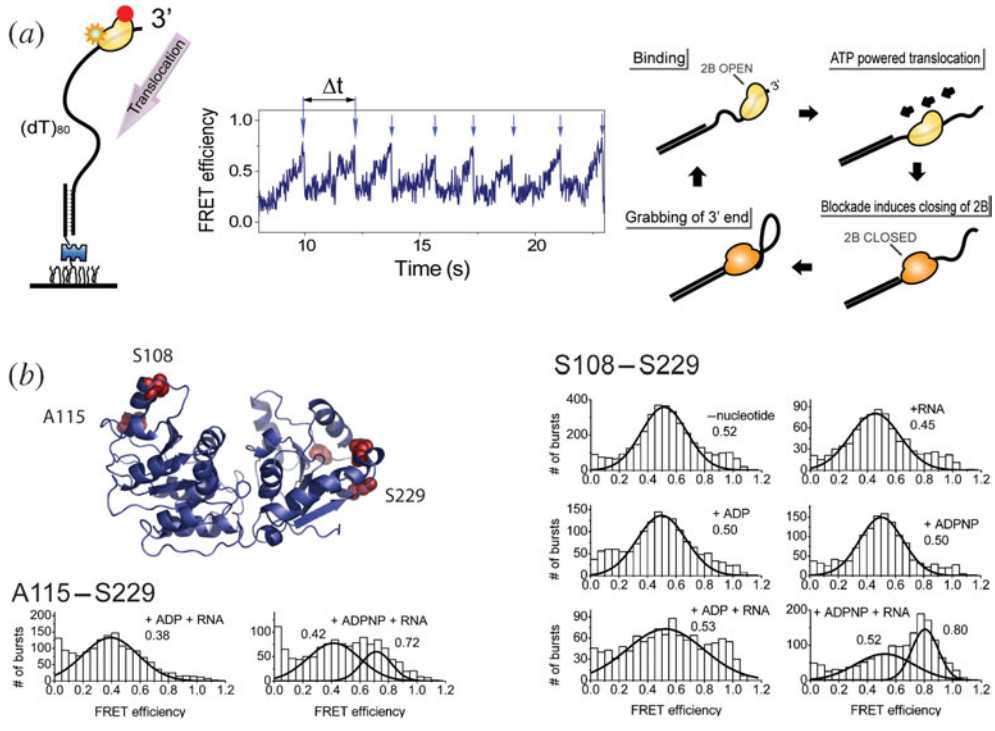


Fig. 6. Single-molecule detection of helicase conformational dynamics. (*a*) From Myong *et al.* (2005). (*Left*) The smFRET assay demonstrates that dual-labeled Rep helicase catalyzes repetitive translocation along unlabeled ssDNA, indicating that Rep itself undergoes a conformational change during the shuttling cycle. (*Right*) Model for the translocation cycle in which Rep transitions from open to closed forms, exposing a secondary binding site for the free 3′ ss tail, allowing Rep to transfer from the junction to the 3′ end and reinitiate the cycle. Reprinted by permission from Macmillan Publishers Ltd: Nature *437*, 1321–1325, copyright (2005). (*b*) From Theissen *et al.* (2008). (*Top left*) Dual fluorescent labeling of YxiN, DEAD-box helicase with donor and acceptor on different sides of the interdomain cleft separating the two RecA-like helicase domains. (*Right*) FRET histograms ± ligands for fluorescently labeled YxiN* S108C/S229C. FRET in the absence of any ligands or in the presence of any individual ligand is 0·5. Cooperative binding of ADPNP and RNA promotes interdomain cleft closure, increasing FRET to 0·8. (*Bottom left*) FRET histograms ± ligands for fluorescently labeled YxiN* A115C/S229C. FRET in the absence of any ligands or in the presence of any individual ligand is 0·42. Cooperative binding of ADPNP and RNA promotes interdomain cleft closure, increasing FRET to 0·72. Adapted from Theissen, B. *et al.* (2008). Copyright (2008). National Academy of Sciences, USA. See text for further details.

3.5.2 Replicative helicase–DNA tail interaction dynamics

smFRET has also been applied to investigate interaction dynamics between replicative helicases and ssDNA tails at the fork (Rothenberg *et al.* 2007). The archaeal minichromosome maintenance protein (MCM) from *Sulfolobus solfataricus* (SsoMCM), a homologue of eukaryotic hexameric MCM replicative helicases, was previously characterized to preferentially unwind Y-shaped substrates with accessible 3′ tails. Using acceptor-labeled SsoMCM and donor-labeled substrates, smFRET was applied (Rothenberg *et al.* 2007) to determine the orientation of MCM along the 3′ tail, and confirm the helicase's preference for fork substrates. Binding of unlabeled SsoMCM to forked substrates with acceptor dye placed at the end of the 5′ tail and donor dye placed at various locations on the 3′ tail increased FRET from low to high, consistent with the idea that

https://doi.org/10.1017/S0033583510000107 Published online by Cambridge University Press

MCM bound the 3′ tail through its central channel while interacting with the 5′ tail through an external site on the protein surface. While MCM bound very stably without dissociating for up to an hour, temporal fluctuations in FRET were also observed with N-terminally acceptor-labeled MCM and the donor-labeled 5′ tail but not with the donor-labeled 3′ tail, indicating a specific dynamic interaction between the helicase and the 5′ tail. This work provided evidence that a replicative helicase may also interact with the non-tracking strand during unwinding, possibly playing a role in substrate specificity, helicase stability at the fork, and unwinding (Rothenberg *et al.* 2007), and suggesting that 'exclusion' of this strand may not be the main mechanistic role.

3.5.3 DEAD-Box RNA helicase conformational switching

Cofactor-induced conformational changes in DEAD-box RNA helicases have also been probed using smFRET-based techniques (Aregger & Klostermeier, 2009; Karow & Klostermeier, 2009; Linden *et al.* 2008; Theissen *et al.* 2008). Crystal structures of members of this helicase family reveal a common core structure consisting of two RecA-like helicase domains separated by an interdomain cleft, and suggest that simultaneous binding of ssRNA and nucleotide induces a conformational change from an 'open' state in which the helicase domains are separated to a 'closed' state in which the helicase domains make multiple contacts with each other. As there is no DEAD-box RNA helicase for which both open and closed structures are available, Klostermeier and co-workers utilized a confocal smFRET method (shown in Fig. 2*b*) to analyze interdomain cleft movement in *Bacillus subtillus* YxiN, a helicase involved in ribosome biogenesis (Theissen *et al.* 2008). YxiN double mutants were constructed for attachment of a donor and an acceptor in each helicase domain. In the absence of ligands, double-labeled YxiN followed a unimodal mid-FRET distribution consistent with a single open conformation. In the presence of nucleotide or RNA alone, the FRET distributions remained unaltered; however, simultaneous addition of ADPNP/ATP plus RNA resulted in a switch to a high FRET species for all the YxiN double mutants. Thus RNA and ATP substrates act cooperatively to induce closure of the interdomain cleft, bringing the helicase domains in close contact (Fig. 6*b*). Thus, smFRET captured both open and closed conformations of YxiN and correlated them with RNA/ADP-bound and RNA/ATP-bound states of the helicase, respectively (Theissen *et al.* 2008). In a follow-up study (Aregger & Klostermeier, 2009), it was shown that YxiN remained in the closed state in the presence of ATP analogues plus RNA, suggesting that helicase reopening post-ATP hydrolysis is most likely coupled to P_i release. Furthermore, YxiN mutants deficient in unwinding were still able to undergo interdomain cleft closure, indicating that cleft closure is important but not sufficient for unwinding (Karow & Klostermeier, 2009). This assay was also applied to investigate the substrate specificity of a related DEAD-box RNA helicase, Hera from *Thermus thermophilus* (Linden *et al.* 2008). Two RNA substrates that were identified by their ability to induce interdomain cleft closure were RNase P RNA and 23S rRNA hairpin 92, suggesting a role for Hera in ribosome biogenesis. These studies illustrate the success of smFRET applications to determining not only conformational changes undergone by these DEAD-box RNA helicases but also information on their cellular functions (Linden *et al.* 2008).

3.6 Helicases working in multiprotein complexes

The sm results described thus far have yielded important information on unwinding/translocation parameters and mechanisms of helicases by themselves. However, *in vivo*, helicases do not work as isolated molecules but in complexes with, for example, replication, recombination

https://doi.org/10.1017/S0033583510000107 Published online by Cambridge University Press

and repair machinery. Thus, it is essential to observe helicases operating in conjunction with their required partners in these processes such as primase, polymerase and ssDNA binding proteins. This section describes recent applications of sm methods toward this goal.

3.6.1 Phage T4 primosome assembly

Sm techniques have been used to probe the assembly of the bacteriophage T4 primosome, comprised of the hexameric helicase (gp41), primase (gp61), ssDNA binding protein (gp32) and accessory helicase loader protein (gp59). This complex works together with DNA polymerase (gp43), which is aided by sliding clamp (gp45) to carry out DNA synthesis as a replisome. While gp41 can bind to forked templates by itself, its binding is stimulated by gp59, which recruits and loads gp41 helicase onto gp32-coated DNA during recombinational replication. Hammes and co-workers determined the order of assembly of primosome components using a combination of ensemble and smFRET techniques (Zhang *et al.* 2005). In this work, all four primosome proteins were single-labeled with donor or acceptor fluorophores and analyzed for interactions between the various proteins in the presence of ssDNA (ensemble FRET) to obtain binding stoichiometries, or with a biotinylated forked DNA containing both leading and lagging strand junctions (smFRET) to prove direct interactions between proteins and the order in which they were required for assembly. The results led to a model in which a 1:1 complex of gp32 and gp59 first forms on forked DNA followed by recruitment of gp41 helicase and its hexamerization. Subsequent ATP hydrolysis by gp41 leads to dissociation of gp32 and gp59. Primase (gp61) then binds to the gp41–DNA complex to complete primosome assembly. Recently, sm photobleaching experiments showed that the hexameric form of gp59 is required for helicase loading (Arumugam *et al.* 2009). The same group has also used this assay to further probe the role of helicase loader (gp59) in initiation of lagging strand replication (Xi *et al.* 2005a, b).

3.6.2 Phage T7, T4 and *E. coli* replisome dynamics

van Oijen and co-workers have used sm flow-stretch techniques to investigate replisome activity in the bacteriophage T7 and *E. coli* systems (Hamdan *et al.* 2007, 2009; Lee *et al.* 2006; Tanner *et al.* 2008, 2009). The experimental set-up is as shown in Fig. 2*c*, in which a forked λ DNA template is tethered to the surface via a ssDNA region at the 5′ end of the lagging strand template; its 3′ end is attached to a tracking bead; and the entire template is subject to laminar flow at $\sim$3 pN. A DNA primer is annealed to the other strand, creating a primer–template junction for leading strand synthesis. Leading strand synthesis by T7 polymerase was measured in this system (Lee *et al.* 2006) by assembling a minimal replisome (helicase–primase (gp4) and thioredoxin–polymerase (trx–gp5)) and monitoring DNA shortening of the ss lagging strand template during fork unwinding/DNA synthesis. The rate of DNA synthesis matched that measured in bulk assays; however, the processivity of DNA synthesis/unwinding in this concerted system was 1–2 orders of magnitude higher relative to that measured with polymerase or helicase alone. When rNTPs were added to this system to enable primase, short pauses during leading strand synthesis trajectories were observed. These were interpreted to reflect pausing of the polymerase while primers were being formed on the lagging strand template. When excess polymerase was additionally added to this system to enable lagging strand synthesis, the pauses were followed by continued shortening of the DNA and then abrupt lengthening. This pattern was interpreted to represent pausing during primer formation followed by the creation and

https://doi.org/10.1017/S0033583510000107 Published online by Cambridge University Press

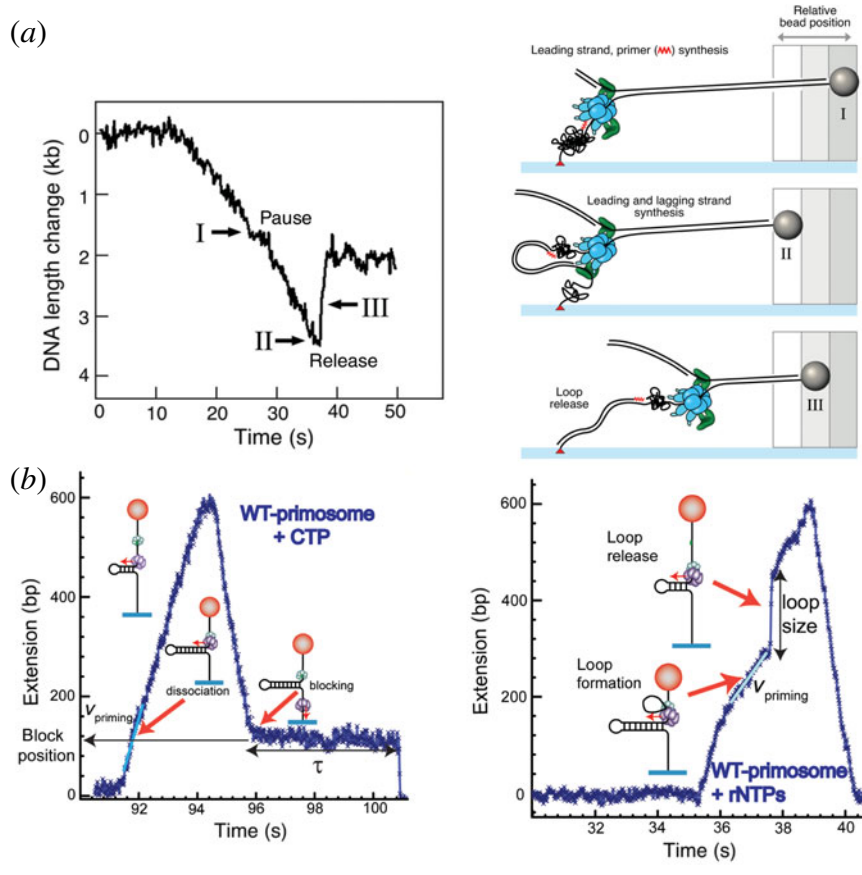


Fig. 7. Single-molecule studies of helicases within replisome complexes. (*a*) From Lee *et al.* (2006). Flow-stretch assay (see Fig. 2*c*) of phage T7 replisome activity monitoring DNA shortening of the lagging strand template generated during leading strand synthesis. Pauses (I) were interpreted to reflect primer synthesis after which lagging strand synthesis continues with the formation of a lagging strand replication loop (II). Loop release (III) is observed as lengthening of the DNA. Reprinted by permission from Macmillan Publishers Ltd: Nature *439*: 621–4, copyright (2006). (*b*) From Manosas *et al.* (2009). Magnetic tweezers assay (see Fig. 2*f*) of phage T4 primosome (gp41 helicase/gp61 primase) activity using a hairpin substrate. Trajectories show an increase in DNA extension representing hairpin unwinding followed by fast or slow (shown) rehybridization (decrease in DNA extension) as helicase continues moving around the hairpin. (*Left*) T4 primosome does not pause while priming (i.e. the unwinding velocity remains constant) and rezipping traces are interrupted by primer-specific periods of constant extension interpreted to represent blocks in reannealing caused by a dissociated primase–primer complex. (*Right*) Detection of priming loop formation in DNA extension time traces represented by periods of slower unwinding velocity followed by jumps back to the original rate reflecting loop release. The priming loop is created by intact primosomes such that the unwound lagging strand template forms a loop that is released upon primer completion and transfer to the lagging strand polymerase. Reprinted by permission from Macmillan Publishers Ltd: Nature Chemical Biology *5*, 904–912, copyright (2009). See text for further details.

release of a DNA loop during lagging strand synthesis (i.e. trombone model). These real-time trajectories of DNA length changes created during action of the minimal T7 replisome were incorporated into a primase-brake model to explain how lagging and leading strand synthesis are synchronized (Lee *et al.* 2006) (Fig. 7*a*).

This flow-stretch assay also confirmed that an electrostatic interaction between the C-terminal tail of the helicase and a basic region in the trx-binding region of the polymerase was crucial for

https://doi.org/10.1017/S0033583510000107 Published online by Cambridge University Press

T7 replisome processivity via retention of trx-gp5 in the event that it dissociates during leading strand synthesis (Hamdan *et al.* 2007). The kinetics of T7 trombone loop formation and dissolution were further analyzed (Hamdan *et al.* 2009), suggesting that the trombone loop is released in response to either new primer formation or Okazaki fragment completion. Loop size also decreased with increasing stretching force, consistent with the idea that the loop is held together by predicted interactions between helicase at the fork and leading and lagging strand polymerases. Imaging of a dsDNA intercalator, YOYO, confirmed that DNA shortening represents both leading and lagging strand formation.

This experimental system was also used to measure primer extension and leading strand synthesis by the *E. coli* PolIII holoenzyme (Tanner *et al.* 2008). Whereas primer extension on an ssDNA template occurred in repeated bursts of ~1 kb separated by pauses, leading strand synthesis on the dsDNA template by the replisome, which also included DnaB, helicase loader DnaC and a minimal clamp loading complex, occurred in ~10 kb increments. The addition of primase (DnaG) decreased the processivity of DNA synthesis 3-fold through its interaction with DnaB, but no pausing was observed suggesting an alternate mechanism for slowing down leading strand synthesis during slow primer synthesis on the lagging strand.

A magnetic tweezers set-up similar to Fig. 2*f* was recently used to monitor phage T4 primosome (i.e. gp41–gp61 helicase–primase) activity on a DNA hairpin substrate (Manosas *et al.* 2009). In this system, unwinding activity is reported as an increase in DNA extension, followed by either rapid rezipping or slow reannealing of the hairpin after helicase dissociation. No pausing was observed during the unwinding phase even when primers are created. Two classes of behavior were observed during primer synthesis. In the first, primase dissociated from the helicase as suggested by periods of no extension during reannealing, which were shown to be caused by transient blocking of hairpin rezipping by the primase–primer complex (Fig. 7*b*). In the second, unwinding traces showed periods of slower velocity unwinding followed by a switch back to the original unwinding rate. This pattern was interpreted to represent the formation of a priming loop by an intact primosome in which the unwound DNA forms a loop between the helicase and primase that is released once the primer is synthesized. The slower unwinding velocity is due to the fact that only one of the two unwound strands contributes to the extension (Fig. 7*b*). A fused primosome (i.e. a single gp41–gp61 polypeptide) worked entirely via the priming loop mechanism, and addition of T4 replisome accessory proteins increased the probability of priming loop formation. This work has thus provided evidence for two types of primosome behavior during primer synthesis involving either primosome disassembly or a priming loop.

A related study on the phage T7 system investigated the coordination of leading/lagging strand synthesis via ensemble and smFRET kinetic assays (Pandey *et al.* 2009). Using smFRET unwinding substrates such as in Fig. 2*a*, and similar radiolabeled substrates for ensemble DNA elongation assays, a primase activity-dependent slowing/pausing was detected during unwinding by gp4 helicase–primase but not during unwinding/DNA synthesis by the T7 replisome, in contrast to previous reports (Lee *et al.* 2006). In a separate experiment, an smFRET substrate with donor placed near the priming sequence and acceptor 40 bp away was utilized to provide evidence for primer-sequence dependent creation of a priming loop during unwinding by both gp4 and the T4 replisome. Finally, ensemble DNA elongation assays showed that lagging strand synthesis is 30% faster than leading strand synthesis by the T4 replisome. Combined, these results suggest three ways of coordinating dual strand synthesis: (1) DNA synthesis occurs concomitantly and is not interrupted by primer synthesis, (2) primase remains engaged with the

https://doi.org/10.1017/S0033583510000107 Published online by Cambridge University Press

priming site during unwinding/DNA synthesis, leading to loop formation in the nascent lagging strand such that the nascent primers are in close proximity for hand-off to the polymerase, and (3) the lagging strand polymerase synthesizes DNA faster, allowing more time for recycling steps and to keep up with leading strand synthesis. In light of this study, prior results that relate pausing during T7 DNA synthesis to primase action (Lee *et al.* 2006) may actually reflect uncoupled lagging and leading strand synthesis.

3.6.3 Effect of human Replication Protein A (hRPA) on BLM unwinding dynamics

The human BLM helicase has been shown to interact with numerous proteins both *in vitro* and *in vivo*. One important partner is the human ssDNA binding protein, replication factor A (hRPA), which facilitates unwinding of long duplex regions by BLM (Brosh *et al.* 2000). This processivity effect was postulated to be due to a direct specific interaction between BLM and hRPA. As described earlier, an smFRET study (Yodh *et al.* 2009) revealed a repetitive unwinding behavior by BLM on forked DNA substrates in which BLM partially unwound a critical length of DNA followed by reversal of unwinding by strand switching, and translocation on the opposing strand with concomitant reannealing of the strands in its wake. After a certain point (i.e. wait time), BLM switched back to the tracking strand and repeated the unwinding cycle. Surprisingly, the repetitive unwinding pattern persisted in the presence of hRPA with only a limited increase in unwinding processivity per cycle. The same effect was observed using the *Saccharomyces cerevisiae* homologue, scRPA, which interacts with BLM through the same residues as hRPA but not with the structurally non-homologous SSB from *E. coli*. This indicated that the hRPA effect is mediated through a direct physical interaction with BLM as opposed to solely hRPA prevention of strand reannealing. The presence of hRPA had no effect on reannealing time, indicating it is most likely dissociating during this phase. And while hRPA did not change the wait time between repetitive unwinding events for wild-type BLM, it did significantly increase the wait time for a mutant BLM that comprises the RecQ helicase core (Janscak *et al.* 2003) but lacks the high-affinity hRPA binding site. The latter result indicates that hRPA facilitates BLM transfer back to the tracking strand and reinitiation of unwinding via direct physical interaction between the two proteins.

3.6.4 Translocation on hRPA-coated DNA by archaeal XPD helicase

Archaeal Rad3 from *Ferroplasma acidarmanus*, a homologue of human XPD helicase required in nucleotide excision repair, possesses a unique Fe–S cluster in helicase domain 1. Spies and co-workers took advantage of the fluorescence quenching property of the Fe–S cluster to examine translocation by this helicase on RPA-coated DNA (Honda *et al.* 2009). *F. acidarmanus* RPA1 and RPA2 have been shown to enhance unwinding by XPD, but whether this is mediated through direct interactions is unknown (Pugh *et al.* 2008). Using short linear ssDNA biotinylated at the 5′ end with Cy3 tethered at the 3′ end, XPD ATP-dependent ssDNA translocation was measured using sm fluorescence microscopy as distance-dependent quenching of Cy3 as a function of time. In the presence of Cy5-labeled RPA1 and RPA2, XPD continued translocation by one of two mechanisms – either with concurrent dissociation of RPA1 or while bypassing RPA2. Both these patterns were confirmed in experiments monitoring Cy5-RPA quenching induced by translocating XPD on unlabeled DNA. These sm experiments thus provide information on the general mechanisms used by DNA repair helicases when encountering substrates coated with ssDNA binding proteins.

https://doi.org/10.1017/S0033583510000107 Published online by Cambridge University Press

4. Conclusions and future directions

It is clear that sm technology is proving to be an extremely relevant tool for probing the mechanism by which helicase motors work. Force- and fluorescence-based experiments have provided support for models in which helicases move in 1 bp/nt increments with rate-limiting events such as unwinding bursts occurring every 3–6 bp, and physical motions such as strand release occurring in larger steps. Measurements of unwinding force- and sequence-dependence have provided a means to determine the degree of duplex destabilization achieved by helicases across superfamilies. Tweezers-based assays and smFRET methods have allowed observations of sequence-specific pausing and spontaneous pausing/reversal during helicase movement as well as the discovery of repetitive translocation/partial unwinding helicase activities. Fluorescence-based methods have yielded new information on conformational dynamics during helicase–NA and helicase subunit interactions. Finally, flow-stretch, tweezers-based and smFRET experiments have enabled the study of helicases as they operate within the primosome and replisome and in conjunction with relevant partners such as RPA.

Ongoing developments in sm techniques such as use of multicolor FRET, fluorescence-force spectroscopy (Joo *et al.* 2008) and improved spatiotemporal resolution in force-based methods will no doubt further advance our understanding of helicase activity in these and other areas of investigation. Examples of questions requiring further elucidation include how helicases operate in multiprotein complexes involved in repair, recombination and RNA metabolism; the physical basis for directional translocation; helicase action on complex substrates such as Holliday junctions, G-quadruplexes and nucleosomes; and catalysis of alternative helicase activities such as NA ss annealing. However, to date, sm methods have only proven useful to determine new activities and kinetic/mechanistic information about helicases *in vitro*. Thus, perhaps the most relevant next direction to take will be the application of sm imaging techniques to study helicase action *in vivo*.

5. Acknowledgements

We thank Jeehae Park for helpful discussions. This work was supported by the National Institute of Health Grant GM065367 (to T.H.) and the Deutsche Forschungsgemeinschaft (DFG SCHL 1896/1-1 (to M.S.)).

6. References

Abbondanzieri, E. A., Greenleaf, W. J., Shaevitz, J. W., Landick, R. & Block, S. M. (2005). Direct observation of base-pair stepping by RNA polymerase. *Nature* **438**, 460–465.

Ali, J. A. & Lohman, T. M. (1997). Kinetic measurement of the step size of DNA unwinding by *Escherichia coli* UvrD helicase. *Science* **275**, 377–380.

Ali, J. A., Maluf, N. K. & Lohman, T. M. (1999). An oligomeric form of *E. coli* UvrD is required for optimal helicase activity. *Journal of Molecular Biology* **293**, 815–834.

Aregger, R. & Klostermeier, D. (2009). The DEAD box helicase YxiN maintains a closed conformation during ATP hydrolysis. *Biochemistry* **48**, 10679–10681.

Arumugam, S. R., Lee, T. H. & Benkovic, S. J. (2009). Investigation of stoichiometry of T4 bacteriophage helicase loader protein (gp59). *Journal of Biological Chemistry* **284**, 29283–29289.

Berger, J. M. (2008). SnapShot: nucleic acid helicases and translocases. *Cell* **134**, 888.

Bertram, R. D., Hayes, C. J. & Soultanas, P. (2002). Vinylphosphonate internucleotide linkages inhibit the activity of PcrA DNA helicase. *Biochemistry* **41**, 7725–7731.

Betterton, M. D. & Julicher, F. (2003). A motor that makes its own track: helicase unwinding of DNA. *Physical Review Letters* **91**, 258103.

https://doi.org/10.1017/S0033583510000107 Published online by Cambridge University Press

Betterton, M. D. & Julicher, F. (2005). Opening of nucleic-acid double strands by helicases: active versus passive opening. *Physical Review E, Statistical, Nonlinear, and Soft Matter Physics* **71**, 011904.

Bianco, P. R., Brewer, L. R., Corzett, M., Balhorn, R., Yeh, Y., Kowalczykowski, S. C. & Baskin, R. J. (2001). Processive translocation and DNA unwinding by individual RecBCD enzyme molecules. *Nature* **409**, 374–378.

Brendza, K. M., Cheng, W., Fischer, C. J., Chesnik, M. A., Niedziela-Majka, A. & Lohman, T. M. (2005). Autoinhibition of *Escherichia coli* Rep monomer helicase activity by its 2B subdomain. *Proceedings of the National Academy of Sciences USA* **102**, 10076–10081.

Brosh Jr., R. M., Li, J. L., Kenny, M. K., Karow, J. K., Cooper, M. P., Kureekattil, R. P., Hickson, I. D. & Bohr, V. A. (2000). Replication protein A physically interacts with the Bloom's syndrome protein and stimulates its helicase activity. *Journal of Biological Chemistry* **275**, 23500–23508.

Chen, Y., Potratz, J. P., Tijerina, P., Del Campo, M., Lambowitz, A. M. & Russell, R. (2008). DEAD-box proteins can completely separate an RNA duplex using a single ATP. *Proceedings of the National Academy of Sciences USA* **105**, 20203–20208.

Cheng, W., Brendza, K. M., Gauss, G. H., Korolev, S., Waksman, G. & Lohman, T. M. (2002). The 2B domain of the *Escherichia coli* Rep protein is not required for DNA helicase activity. *Proceedings of the National Academy of Sciences USA* **99**, 16006–16011.

Cheng, W., Dumont, S., Tinoco Jr., I. & Bustamante, C. (2007). NS3 helicase actively separates RNA strands and senses sequence barriers ahead of the opening fork. *Proceedings of the National Academy of Sciences USA* **104**, 13954–13959.

Delagoutte, E. & von Hippel, P. H. (2001). Molecular mechanisms of the functional coupling of the helicase (gp41) and polymerase (gp43) of bacteriophage T4 within the DNA replication fork. *Biochemistry* **40**, 4459–4477.

Dessinges, M. N., Lionnet, T., Xi, X. G., Bensimon, D. & Croquette, V. (2004). Single-molecule assay reveals strand switching and enhanced processivity of UvrD. *Proceedings of the National Academy of Sciences USA* **101**, 6439–6444.

Dillingham, M. S., Wigley, D. B. & Webb, M. R. (2000). Demonstration of unidirectional single-stranded DNA translocation by PcrA helicase: measurement of step size and translocation speed. *Biochemistry* **39**, 205–212.

Dillingham, M. S., Wigley, D. B. & Webb, M. R. (2002). Direct measurement of single-stranded DNA translocation by PcrA helicase using the fluorescent base analogue 2-aminopurine. *Biochemistry* **41**, 643–651.

Dohoney, K. M. & Gelles, J. (2001). Chi-sequence recognition and DNA translocation by single RecBCD helicase/nuclease molecules. *Nature* **409**, 370–374.

Dong, F., Weitzel, S. E. & von Hippel, P. H. (1996). A coupled complex of T4 DNA replication helicase (gp41) and polymerase (gp43) can perform rapid and processive DNA strand-displacement synthesis. *Proceedings of the National Academy of Sciences USA* **93**, 14456–14461.

Donmez, I. & Patel, S. S. (2006). Mechanisms of a ring shaped helicase. *Nucleic Acids Research* **34**, 4216–4224.

Dumont, S., Cheng, W., Serebrov, V., Beran, R. K., Tinoco, Jr., I., Pyle, A. M. & Bustamante, C. (2006). RNA translocation and unwinding mechanism of HCV NS3 helicase and its coordination by ATP. *Nature* **439**, 105–108.

Enemark, E. J. & Joshua-Tor, L. (2008). On helicases and other motor proteins. *Current Opinion in Structural Biology* **18**, 243–257.

Essevaz-Roulet, B., Bockelmann, U. & Heslot, F. (1997). Mechanical separation of the complementary strands of DNA. *Proceedings of the National Academy of Sciences USA* **94**, 11935–11940.

Fan, H. F. & Li, H. W. (2009). Studying RecBCD helicase translocation along Chi-DNA using tethered particle motion with a stretching force. *Biophysical Journal* **96**, 1875–1883.

Fischer, C. J. & Lohman, T. M. (2004). ATP-dependent translocation of proteins along single-stranded DNA: models and methods of analysis of pre-steady state kinetics. *Journal of Molecular Biology* **344**, 1265–1286.

Fischer, C. J., Maluf, N. K. & Lohman, T. M. (2004). Mechanism of ATP-dependent translocation of *E. coli* UvrD monomers along single-stranded DNA. *Journal of Molecular Biology* **344**, 1287–1309.

Ha, T. (2007). Need for speed: mechanical regulation of a replicative helicase. *Cell* **129**, 1249–1250.

Ha, T., Rasnik, I., Cheng, W., Babcock, H. P., Gauss, G. H., Lohman, T. M. & Chu, S. (2002). Initiation and re-initiation of DNA unwinding by the *Escherichia coli* Rep helicase. *Nature* **419**, 638–641.

Hamdan, S. M., Johnson, D. E., Tanner, N. A., Lee, J. B., Qimron, U., Tabor, S., van Oijen, A. M. & Richardson, C. C. (2007). Dynamic DNA helicase–DNA polymerase interactions assure processive replication fork movement. *Molecular Cell* **27**, 539–549.

Hamdan, S. M., Loparo, J. J., Takahashi, M., Richardson, C. C. & van Oijen, A. M. (2009). Dynamics of DNA replication loops reveal temporal control of lagging-strand synthesis. *Nature* **457**, 336–339.

Handa, N., Bianco, P. R., Baskin, R. J. & Kowalczykowski, S. C. (2005). Direct visualization of RecBCD movement reveals cotranslocation of the RecD motor after chi recognition. *Molecular Cell* **17**, 745–750.

Henn, A., Medalia, O., Shi, S. P., Steinberg, M., Franceschi, F. & Sagi, I. (2001). Visualization of unwinding activity of duplex RNA by DbpA, a DEAD box helicase, at single-molecule resolution by atomic

https://doi.org/10.1017/S0033583510000107 Published online by Cambridge University Press

force microscopy. *Proceedings of the National Academy of Sciences USA* **98**, 5007–5012.

Hilbert, M., Karow, A. R. & Klostermeier, D. (2009). The mechanism of ATP-dependent RNA unwinding by DEAD box proteins. *Biological Chemistry* **390**, 1237–1250.

Honda, M., Park, J., Pugh, R. A., Ha, T. & Spies, M. (2009). Single-molecule analysis reveals differential effect of ssDNA-binding proteins on DNA translocation by XPD helicase. *Molecular Cell* **35**, 694–703.

Hopfner, K. P. & Michaelis, J. (2007). Mechanisms of nucleic acid translocases: lessons from structural biology and single-molecule biophysics. *Current Opinion in Structural Biology* **17**, 87–95.

Jankowsky, E., Gross, C. H., Shuman, S. & Pyle, A. M. (2000). The DExH protein NPH-II is a processive and directional motor for unwinding RNA. *Nature* **403**, 447–451.

Janscak, P., Garcia, P. L., Hamburger, F., Makuta, Y., Shiraishi, K., Imai, Y., Ikeda, H. & Bickle, T. A. (2003). Characterization and mutational analysis of the RecQ core of the bloom syndrome protein. *Journal of Molecular Biology* **330**, 29–42.

Johnson, D. S., Bai, L., Smith, B. Y., Patel, S. S. & Wang, M. D. (2007). Single-molecule studies reveal dynamics of DNA unwinding by the ring-shaped T7 helicase. *Cell* **129**, 1299–1309.

Joo, C., Balci, H., Ishitsuka, Y., Buranachai, C. & Ha, T. (2008). Advances in single-molecule fluorescence methods for molecular biology. *Annual Review of Biochemistry* **77**, 51–76.

Karow, A. R. & Klostermeier, D. (2009). A conformational change in the helicase core is necessary but not sufficient for RNA unwinding by the DEAD box helicase YxiN. *Nucleic Acids Research* **37**, 4464–4471.

Lee, J. B., Hite, R. K., Hamdan, S. M., Xie, X. S., Richardson, C. C. & van Oijen, A. M. (2006). DNA primase acts as a molecular brake in DNA replication. *Nature* **439**, 621–624.

Lee, J. Y. & Yang, W. (2006). UvrD helicase unwinds DNA one base pair at a time by a two-part power stroke. *Cell* **127**, 1349–1360.

Linden, M. H., Hartmann, R. K. & Klostermeier, D. (2008). The putative RNase P motif in the DEAD box helicase Hera is dispensable for efficient interaction with RNA and helicase activity. *Nucleic Acids Research* **36**, 5800–5811.

Lionnet, T., Dawid, A., Bigot, S., Barre, F. X., Saleh, O. A., Heslot, F., Allemand, J. F., Bensimon, D. & Croquette, V. (2006). DNA mechanics as a tool to probe helicase and translocase activity. *Nucleic Acids Research* **34**, 4232–4244.

Lionnet, T., Spiering, M. M., Benkovic, S. J., Bensimon, D. & Croquette, V. (2007). Real-time observation of bacteriophage T4 gp41 helicase reveals an unwinding mechanism. *Proceedings of the National Academy of Sciences USA* **104**, 19790–19795.

Liu, F., Putnam, A. & Jankowsky, E. (2008). ATP hydrolysis is required for DEAD-box protein recycling but not for duplex unwinding. *Proceedings of the National Academy of Sciences USA* **105**, 20209–20214.

Lohman, T. M. & Bjornson, K. P. (1996). Mechanisms of helicase-catalyzed DNA unwinding. *Annual Review of Biochemistry* **65**, 169–214.

Lohman, T. M., Tomko, E. J. & Wu, C. G. (2008). Non-hexameric DNA helicases and translocases: mechanisms and regulation. *Nature Reviews Molecular Cell Biology* **9**, 391–401.

Lucius, A. L., Maluf, N. K., Fischer, C. J. & Lohman, T. M. (2003). General methods for analysis of sequential "n-step" kinetic mechanisms: application to single turnover kinetics of helicase-catalyzed DNA *unwinding*. *Biophysical Journal* **85**, 2224–2239.

Lucius, A. L., Vindigni, A., Gregorian, R., Ali, J. A., Taylor, A. F., Smith, G. R. & Lohman, T. M. (2002). DNA unwinding step size of *E. coli* RecBCD helicase determined from single turnover chemical quenched-flow kinetic studies. *Journal of Molecular Biology* **324**, 409–428.

Maluf, N. K., Fischer, C. J. & Lohman, T. M. (2003). A dimer of *Escherichia coli* UvrD is the active form of the helicase *in vitro*. *J. Mol. Biol.* **325**, 913–935.

Manosas, M., Spiering, M. M., Zhuang, Z., Benkovic, S. J. & Croquette, V. (2009). Coupling DNA unwinding activity with primer synthesis in the bacteriophage T4 primosome. *Nature Chemical Biology* **5**, 904–912.

Marsden, S., Nardelli, M., Linder, P. & McCarthy, J. E. (2006). Unwinding single RNA molecules using helicases involved in eukaryotic translation initiation. *Journal of Molecular Biology* **361**, 327–35.

Moffitt, J. R., Chemla, Y. R., Aathavan, K., Grimes, S., Jardine, P. J., Anderson, D. L. & Bustamante, C. (2009). Intersubunit coordination in a homomeric ring ATPase. *Nature* **457**, 446–450.

Myong, S., Bruno, M. M., Pyle, A. M. & Ha, T. (2007). Spring-loaded mechanism of DNA unwinding by hepatitis C virus NS3 helicase. *Science* **317**, 513–516.

Myong, S., Cui, S., Cornish, P. V., Kirchhofer, A., Gack, M. U., Jung, J. U., Hopfner, K. P. & Ha, T. (2009). Cytosolic viral sensor RIG-I is a 5′-triphosphate-dependent translocase on double-stranded RNA. *Science* **323**, 1070–1074.

Myong, S., Rasnik, I., Joo, C., Lohman, T. M. & Ha, T. (2005). Repetitive shuttling of a motor protein on DNA. *Nature* **437**, 1321–1325.

Niedziela-Majka, A., Chesnik, M. A., Tomko, E. J. & Lohman, T. M. (2007). *Bacillus stearothermophilus* PcrA monomer is a single-stranded DNA translocase but not a processive helicase *in vitro*. *Journal of Biological Chemistry* **282**, 27076–27085.

https://doi.org/10.1017/S0033583510000107 Published online by Cambridge University Press

Pandey, M., Syed, S., Donmez, I., Patel, G., Ha, T. & Patel, S. S. (2009). Coordinating DNA replication by means of priming loop and differential synthesis rate. *Nature* **462**, 940–943.

Patel, S. S. & Donmez, I. (2006). Mechanisms of helicases. *Journal of Biological Chemistry* **281**, 18265–18268.

Perkins, T. T., Li, H. W., Dalal, R. V., Gelles, J. & Block, S. M. (2004). Forward and reverse motion of single RecBCD molecules on DNA. *Biophysical Journal* **86**, 1640–1648.

Phillips, R., Kondev, J. & Theriot, J. (2008). *Physical Biology of the Cell*. New York, NY: Garland Science, Taylor & Francis Group.

Pugh, R. A., Lin, Y., Eller, C., Leesley, H., Cann, I. K. & Spies, M. (2008). Ferroplasma acidarmanus RPA2 facilitates efficient unwinding of forked DNA substrates by monomers of FacXPD helicase. *Journal of Molecular Biology* **383**, 982–998.

Pyle, A. M. (2008). Translocation and unwinding mechanisms of RNA and DNA helicases. *Annual Review of Biophysics* **37**, 317–336.

Ramanathan, S. P., van Aelst, K., Sears, A., Peakman, L. J., Diffin, F. M., Szczelkun, M. D. & Seidel, R. (2009). Type III restriction enzymes communicate in 1D without looping between their target sites. *Proceedings of the National Academy of Sciences USA* **106**, 1748–1753.

Rasnik, I., Myong, S. & Ha, T. (2006). Unraveling helicase mechanisms one molecule at a time. *Nucleic Acids Research* **34**, 4225–4231.

Ratcliff, G. C. & Erie, D. A. (2001). A novel single-molecule study to determine protein–protein association constants. *Journal of the American Chemical Society* **123**, 5632–5635.

Rothenberg, E., Trakselis, M. A., Bell, S. D. & Ha, T. (2007). MCM forked substrate specificity involves dynamic interaction with the 5′-tail. *Journal of Biological Chemistry* **282**, 34229–34234.

Roy, R., Hohng, S. & Ha, T. (2008). A practical guide to single-molecule FRET. *Nature Methods* **5**, 507–516.

Schrock, R. D. & Alberts, B. (1996). Processivity of the gene 41 DNA helicase at the bacteriophage T4 DNA replication fork. *Journal of Biological Chemistry* **271**, 16678–16682.

Serebrov, V., Beran, R. K. & Pyle, A. M. (2009). Establishing a mechanistic basis for the large kinetic steps of the NS3 helicase. *Journal of Biological Chemistry* **284**, 2512–2521.

Serebrov, V. & Pyle, A. M. (2004). Periodic cycles of RNA unwinding and pausing by hepatitis C virus NS3 helicase. *Nature* **430**, 476–480.

Singleton, M. R., Dillingham, M. S. & Wigley, D. B. (2007). Structure and mechanism of helicases and nucleic acid translocases. *Annual Review of Biochemistry* **76**, 23–50.

Singleton, M. R. & Wigley, D. B. (2002). Modularity and specialization in superfamily 1 and 2 helicases. *Journal of Bacteriology* **184**, 1819–1826.

Slatter, A. F., Thomas, C. D. & Webb, M. R. (2009). PcrA helicase tightly couples ATP hydrolysis to unwinding double-stranded DNA, modulated by the initiator protein for plasmid replication, RepD. *Biochemistry* **48**, 6326–6334.

Spies, M., Amitani, I., Baskin, R. J. & Kowalczykowski, S. C. (2007). RecBCD enzyme switches lead motor subunits in response to chi recognition. *Cell* **131**, 694–705.

Spies, M., Bianco, P. R., Dillingham, M. S., Handa, N., Baskin, R. J. & Kowalczykowski, S. C. (2003). A molecular throttle: the recombination hotspot chi controls DNA translocation by the RecBCD helicase. *Cell* **114**, 647–654.

Stano, N. M., Jeong, Y. J., Donmez, I., Tummalapalli, P., Levin, M. K. & Patel, S. S. (2005). DNA synthesis provides the driving force to accelerate DNA unwinding by a helicase. *Nature* **435**, 370–373.

Sun, B., Wei, K. J., Zhang, B., Zhang, X. H., Dou, S. X., Li, M. & Xi, X. G. (2008). Impediment of *E. coli* UvrD by DNA-destabilizing force reveals a strained-inchworm mechanism of DNA unwinding. *EMBO Journal* **27**, 3279–3287.

Tanner, N. A., Hamdan, S. M., Jergic, S., Loscha, K. V., Schaeffer, P. M., Dixon, N. E. & van Oijen, A. M. (2008). Single-molecule studies of fork dynamics in *Escherichia coli* DNA replication. *Nature Structural and Molecular Biology* **15**, 170–176.

Tanner, N. A., Loparo, J. J., Hamdan, S. M., Jergic, S., Dixon, N. E. & van Oijen, A. M. (2009). Real-time single-molecule observation of rolling-circle DNA replication. *Nucleic Acids Research* **37**, e27.

Theissen, B., Karow, A. R., Kohler, J., Gubaev, A. & Klostermeier, D. (2008). Cooperative binding of ATP and RNA induces a closed conformation in a DEAD box RNA helicase. *Proceedings of the National Academy of Sciences USA* **105**, 548–553.

Tomko, E. J., Fischer, C. J., Niedziela-Majka, A. & Lohman, T. M. (2007). A nonuniform stepping mechanism for *E. coli* UvrD monomer translocation along single-stranded DNA. *Molecular Cell* **26**, 335–347.

Velankar, S. S., Soultanas, P., Dillingham, M. S., Subramanya, H. S. & Wigley, D. B. (1999). Crystal structures of complexes of PcrA DNA helicase with a DNA substrate indicate an inchworm mechanism. *Cell* **97**, 75–84.

Wickersham, C. E., Cash, K. J., Pfeil, S. H., Bruck, I., Kaplan, D. L., Plaxco, K. W. & Lipman, E. A. (2010). Tracking a molecular motor with a nanoscale optical encoder. *NanoLetters*, **10**(3), 1022–1027.

Xi, J., Zhang, Z., Zhuang, Z., Yang, J., Spiering, M. M., Hammes, G. G. & Benkovic, S. J. (2005a). Interaction between the T4 helicase loading protein (gp59) and the

https://doi.org/10.1017/S0033583510000107 Published online by Cambridge University Press

DNA polymerase (gp43): unlocking of the gp59–gp43–DNA complex to initiate assembly of a fully functional replisome. *Biochemistry* **44**, 7747–7756.

Xi, J., Zhuang, Z., Zhang, Z., Selzer, T., Spiering, M. M., Hammes, G. G. & Benkovic, S. J. (2005b). Interaction between the T4 helicase-loading protein (gp59) and the DNA polymerase (gp43): a locking mechanism to delay replication during replisome assembly. *Biochemistry* **44**, 2305–2318.

Yang, Y., Dou, S. X., Ren, H., Wang, P. Y., Zhang, X. D., Qian, M., Pan, B. Y. & Xi, X. G. (2008). Evidence for a functional dimeric form of the PcrA helicase in DNA unwinding. *Nucleic Acids Research* **36**, 1976–1989.

Yodh, J. G., Stevens, B. C., Kanagaraj, R., Janscak, P. & Ha, T. (2009). BLM helicase measures DNA unwound before switching strands and hRPA promotes unwinding reinitiation. *EMBO Journal* **28**, 405–416.

Zhang, W., Dillingham, M. S., Thomas, C. D., Allen, S., Roberts, C. J. & Soultanas, P. (2007). Directional loading and stimulation of PcrA helicase by the replication initiator protein RepD. *Journal of Molecular Biology* **371**, 336–348.

Zhang, Z., Spiering, M. M., Trakselis, M. A., Ishmael, F. T., Xi, J., Benkovic, S. J. & Hammes, G. G. (2005). Assembly of the bacteriophage T4 primosome: single-molecule and ensemble studies. *Proceedings of the National Academy of Sciences USA* **102**, 3254–3259.

https://doi.org/10.1017/S0033583510000107 Published online by Cambridge University Press